UNIVERSITY OF TARTU

Faculty of science and technology

Institute of physics

Synthesis of silver and cerium dioxide nanoparticles and study of their antiviral activity

Stevin Lilla

Masters' thesis (30 ECTS)

Supervisors:

Tanel Tätte

Alexander Vanetsev

Tartu 2021

Synthesis of silver and cerium dioxide nanoparticles and study of their antiviral activity

In this work colloidal silver and ceria nanoparticles were synthesized, characterized and tested as antiviral materials. Both particles size, size distribution and surface conditions were studied using various methods, including TEM and SEM analysis, DLS/zeta-potential measurements, UV-Vis and IR spectroscopy. Approaches to distribute synthesized particles on the porous surfaces were developed and tested.

Effects of silver and CeO_2 nanoparticles on model bioactive compounds (amino acids and BSA protein) are studied. It was shown, that the action of silver nanoparticles is mainly connected with the dissolved Ag^+ ions, while the action of CeO_2 nanoparticles is of a more complex nature, affecting the structure of the treated compounds, and requires additional investigations.

Antiviral properties were studied by measuring infectivity of influenza virus A/WSN/1933 (H1N1) using plaque assay. CeO_2 particles showed a significant antiviral effect with close to zero cytotoxicity.

Keywords: nanoparticles; silver; cerium dioxide; synthesis; antiviral properties; colloidal solutions

CERCS codes and names: T150 – Materials Technology, P360 - Inorganic chemistry

Hõbeda ja tseeriumdioksiidi süntees ja nende antiviraalsed omadused.

Käesolevas töös sünteesiti ja karakteriseeriti hõbeda ja tseeriumdioksiidi nanoosakesi ning uuriti nende viirustevastaseid omadusi. Osakeste suurusi, suuruste jaotust ja pinna omadusi uuriti kasutades erinevaid meetodeid – SEM ja TEM analüüsi, DLS/zeta-potentsiaali mõõtmisi, UV-Vis ja infrapuna spektroskoopiat. Uuriti sünteesitud osakeste seostumist poorsetele pindadele.

Uuriti hõbeda ja CeO_2 mõju bioaktiivsuse mudelmolekulidele (aminohapped ja BSA valk). Hõbeda nanoosakeste mõju uuritud osakestele seletati peamiselt nanoosakestelt lahustunud Ag^+-ioonide mõjuga. CeO_2 osakeste mõju mehhanism osutus keerulisemaks. Näidati, et need mõjutavad kokkupuutes mudelühendite struktuuri. Mõju täpsem mehhanism vajab aga edasist uurimist.

Viirusevastased toimeid uuriti mõõtes gripiviiruse A/WSN/1933 (H1N1) nakatuvust kasutades plaagidepõhist analüüsi. CeO_2 osakestel oli tugev viirusevastane toime sama aegselt peaaegu olematu tsütotoksilisusega.

Märksõnad:

CERCS kood ja nimetus: T150 – Materjalitehnoloogia, P360 – Anorgaaniline keemia

Contents

Used acronyms 6

Introduction 7

1. Literature review 9

1.1. Silver nanoparticles 9

1.2. Cerium oxide nanoparticles 12

1.3. Spectroscopical analysis of amino acids and proteins and their interaction with nanoparticles 16

1.3.1. Infrared spectroscopy 16

1.3.2. Luminescence and CD spectroscopy 17

2. Experimental 20

2.1. Silver nanoparticles synthesis 20

2.2. Ceria nanoparticles synthesis 21

2.3. Methods of analysis. 22

3. Results and discussion 24

3.1. Nanoparticle morphology 24

3.2. Distribution of synthesized nanoparticles on the surfaces 30

3.3. Study of the effect of synthesized nanoparticles on model amino acids and BSA protein. 32

3.3.1. IR and luminescent spectroscopy of amino acids after treatment with synthesized nanoparticles 32

3.3.2. BSA protein measurements after treatment with positively charged CeO_2 nanoparticles 45

3.4. Antiviral testing of synthesized nanoparticles 46

4. Conclusions 51

5. Kokkuvõte 52

Author's contribution 53

Acknowledgements 53

References 54

Lihtlitsents lõputöö reprodutseerimiseks ja üldsusele kättesaadavaks tegemiseks. 61

Mina, Stevin Lilla, ... 61

Used acronyms

IR	Infrared
ROS	Reactive oxygen species
ATR	Attenuated total reflection
BSA	Bovine serum albumin
PVP	Polyvinylpyrrolidone
SEM	Scanning electron microscope
TEM	Transmission electron microscope
UV-Vis	ultraviolet – visual spectrophotometry
DLS	Dynamic light scattering
CD	Circular dichroism
HMTA	Hexamethylenetetramine
NATA	N-acetyl tryptophan amide
HTMW	Hydrothermal microwave

Introduction

Because of the outbreak of SARS-CoV-2, scientists all over the globe are looking for ways to contain and stop the spread of viruses, both existing today and in the future. Currently main methods to fight against virus infection is preventative measures, like disinfecting surfaces or wearing masks, and antiviral drugs, which inhibit virus development. One of the ways to combat the spread of the virus can be application of nanoscale materials. Nanoparticles have been widely used in many different medical applications, such as contrast agents in imaging, drug and gene delivery agents into specific organs or tumors, and localized heating for hyperthermal therapy. Nanoparticles have also been used as antiviral agents [1], [2]. However, most of the nanoparticles have little potential as an antiviral drug for internal usage. More promising is external treatment of various objects and commonly used surfaces with antivirally efficient nanoparticles, similarly to current disinfection of surfaces with antiseptics.

One of the most well-known antimicrobial nanomaterials is silver. Silver nanoparticles have been widely reported as having antimicrobial properties against bacteria, fungi and viruses. Silver particles are already used in many different products, such as wound dressings, deodorant sprays and various fabrics. Besides silver there are other metal particles that may exhibit antiviral properties. Another promising material for antiviral applications is nanocrystalline CeO_2. It is much less studied in biological applications than silver, however some resent works indicate that CeO_2 could be used as an antiviral agent, harmless for people [3].

It is important to find an optimal method of synthesis, that provides us with particles with the largest efficiency against viruses. The synthesis method should also be simple and scalable for mass production. The synthesized particles should not be harmful to humans, so cytotoxicity to mammalian cells should also be studied.

Our goal was to synthesize silver and CeO_2 nanoparticles, uniform in morphology, disaggregated and stable in aqueous colloids, and study their functional properties with both model systems and real viruses. Distribution of synthesized nanoparticles on porous surfaces was also performed. Amino acids and BSA protein were used as models to study chemical effect of synthesized nanoparticles on biological systems, due to the fact that

real viruses are too complex systems for spectroscopical analysis. Plaque based assays were used to study activity of the nanoparticles against virus A/WSN/1933 (H1N1), which is a strain of human influenza A virus.

The main body of work was performed in the Institute of Physics, University of Tartu, whilst experiments with viruses were performed in the Institute of Technology, University of Tartu.

1. Literature review

1.1. Silver nanoparticles

Silver nanoparticles, as many other nanosized objects, have unique electrical, magnetic and optical properties that are very different from a bulk material and depend on the size and shape of the particles [4].This is known as the size effect. These effects happen in nanoscale, because properties of surface atoms are different from atoms in rest of the material, and in nanoparticles, the surface is a larger portion of the whole material. Therefore, surface atoms have a much greater effect on chemical and physical properties of the nanoparticles. There are many different size effects that can appear in nanomaterials such as: thermal, mechanical, kinetic, electrical, magnetic, optical and chemical. Nano size effects that are particularly studied are surface plasmon resonance, catalytical and antimicrobial effects. Surface plasmon resonance happens in particles, because the particles are surrounded by an electron cloud, which can resonate with incoming light (Fig. 1). The size of the particle directly influences surface plasmon resonance wavelength and with it, the color of the colloid solution [5]. Generally, the larger the particle, the longer the wavelength of light that is absorbed.

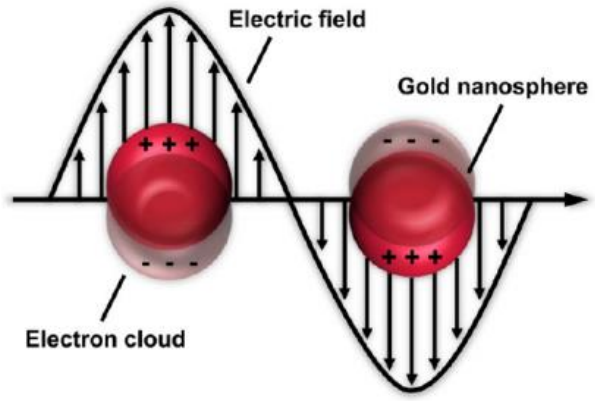

Figure 1. Schematic of localized surface plasmon resonance on gold nanospheres [6].

Many anoparticles are known to be stable in another phase in a form of so called colloid solution or sol. A colloid is a nanoscale homogeneous mixture in which a microscopically small substance in one phase is suspended throughout another substance in a different phase. Commonly found example would be solid nanoparticles suspended in a liquid solution. The colloid system remains stable when the particles remain suspended in

solution. This is dependent on the interaction between particles. Electrostatic and steric stabilization are the two main mechanisms for stabilizing colloid solutions. Electrostatic stabilization is based on mutual repulsion of electrical charges. The suspended particles are surrounded by an electric double layer. The particles are charged on the surface and attract an oppositely charged ion, which surrounds the particle. The electrostatic repulsion between suspended colloidal particles is known as zeta potential.

There are many different methods to synthesize silver nanoparticles, from straight-forward chemical reduction of silver salt solutions and seed-mediated synthesis to photochemical reduction, and electrochemical approaches. The most widely used methods are based on the reduction of metal salts. A soluble silver salt is mixed together with a reducing agent and a capping agent or surfactant. Capping agents and surfactants hinder the growth and aggregation of silver crystal. Sometimes capping agent and reducing reagent is the same compound. Typical reducing agents are various organic compounds and soluble borohydrides or alumohydrates. Capping and stabilizing agents are also various organic compounds.

One of the simplest and yet very efficient variations of the salt reduction pathways of silver nanoparticles synthesis is a modification of the well-known Turkevich method for gold nanoparticles synthesis, in which sodium citrate acts as both the reducing and capping agent [7]. This method produces 20 nm to 200 nm silver particles with a wide range of shapes. In the synthesis process, dissolved silver ions get reduced by citrate ions and which also absorb to the surface of growing particles preventing them from aggregation. This leads to the formation of stable aqueous colloids of citrate-capped silver nanoparticles. The varying size and shape of the silver particles happens because of the continuous nucleation and growth in the solution throughout the whole synthetic process [8]. Using simple citrate reduction method results in highly variable sized particles. To achieve more uniform morphology in the particle, more complex approaches are used.

One of the ways to synthesize nanoparticles with a controllable size and shape is a seed-mediated growth. This approach introduces a two-stage formation scheme. On the first stage a strong reducing agent (e.g., sodium borohydride) in an extremely diluted solution of a silver salt is used to create ultra-small (2-5 nm) metal nanoparticles – “seeds”. On

the second stage “seeds”, together with a softer reducing agent (e.g. citric acid or PVP) and silver salt in higher concentration, are used to promote controllable growth of nanoparticles in mild conditions. This method, due to separation of nucleation and growth stages, results in narrower size distribution and more uniform shape of the nanoparticles [9]. And the more uniform morphology of synthesized nanoparticles ensures their more reproducible properties in various applications, including biomedical.

The larger surface to volume of the particles contributes to higher chance of dissolving ions into the solution, which leads to higher reactivity. These ions can then react with different functional groups in biological systems and can lead to antimicrobial effects. Antimicrobial properties of silver have been observed for a long time. Silver particles have been added to many products like bandages, textiles and other household items. Cytotoxic properties can be dependent of the morphology of the particles. Studies have shown that nano-sized silver is more effective as a bacterial biocide. Silver particles in contact with E. coli bacteria led to holes in cell membranes and cell death. The main reasons for this were thought to be silver ions reacting with protein functional groups, to disrupt bacterial cells [10]. The exact mechanism leading to cell death is yet not completely clear, since there are many competing ways in which cell death can occur.

One of the first hypotheses was that the silver particles accumulate on the surface of bacterial cells, where they react to cause holes and lead to cell death. This is now considered unlikely, since particles with different sizes all exhibit antibacterial properties, so it’s more likely there is a secondary specie, coming from the particle [11]. One of such specie is considered to be different oxygen radicals, also called reactive oxygen species (ROS). ROS are generated during metabolism in all cells. With the addition of silver particles production of ROS is increased, especially highly toxic hydroxyl radicals. The amount of ROS in bacterial cells has been measured in both aerobic and anaerobic conditions after adding silver particles, and was comparatively larger in aerobic conditions [12]. Therefore, it is likely that silver particles are generating ROS inside bacteria in aerobic conditions. One such generation mechanism is presented in Fig. 2.

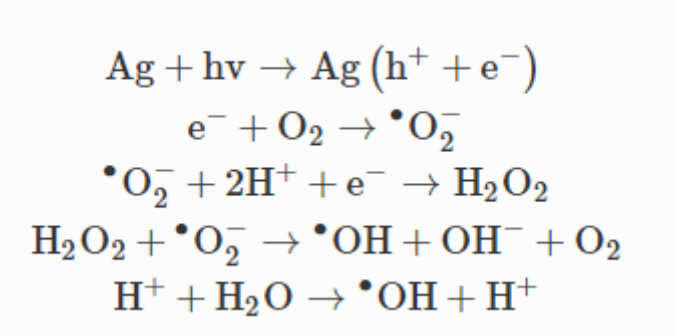

Figure 2. Suggested mechanism of ROS generation [12].

The other prominent species that cause bacterial cell death are silver ions. Silver ions possess a high affinity for organic amines, phosphates and thiols. Ions reacting with these functional groups leads to irreversible bonding and aggregation of molecules. Several of the molecules, like DNA or peptides in the membrane have been shown to be targets of silver ions and can be explained as a reason for cell death. Since silver ions lack selectivity, it is unlikely that a single pathway is causing cell death. It is more likely silver ions bind to many different targets and disrupts many aspects of cell metabolism [13]. The variety of mechanisms of action for silver nanoparticles and their relatively low toxicity for human organisms make their use very attractive in biomedical applications.

1.2. Cerium oxide nanoparticles

Cerium is a rare earth metal that forms an oxide with a face centered fluorite crystalline structure. Applications of ceria have been as catalysts, fuel additives, high temperatural solid oxide fuel cell electrolytes, solar cells and others. Recently, cerium oxide particles have generated interest in biomedical science for its unique properties. The crystal structure of ceria has oxygen vacancies as defects, which are amplified by particle size-effects. The vacancies are formed from the ox-redox transition between Ce^{4+} and Ce^{3+} oxidation states ceria nanoparticles ceria nanoparticles in ceria. This effect is more pronounced in cerium oxide nanoparticles, which have a larger concentration of Ce^{3+} instead of Ce^{4+}, which are more prevalent in bulk oxide. Reduction in particle size leads to increased fraction of atoms on the surface and reduction in surface atom coordination [14]. Nonstoichiometry of anion sublattice defines many of the functional properties of cerium dioxide from ionic conductivity to the bioactivity. In particular, oxygen vacancies

can help to reduce oxidative stress from ROS and free radicals when ceria nanoparticles are introduced into a biosystem [15]. This radical scavenging effect is active in healthy cells, which have physiological pH levels. On the other hand, in more acidic than physiological conditions, such as some cancer cells or bacteria, ceria nanoparticles can also generate ROS. [16]. When nanoceria interacts with bacterial cells by electrostatic attractions, ROS is generated, which can lead to bacterial cell death [17], [18]. There seems to be dependence of antioxidant activities on particle size.. Smaller particles have larger surface area and therefore relatively more vacancies [19].

There are many different methods to synthesize ceria nanoparticles. These can broadly be classified as hydrolysis, hydrothermal treatment, synthesis in microemulsions, oxidation and so-called green methods. Green methods are usually a modification of one of the previously listed techniques, but there is more consideration towards reducing harmful effects and toxic chemicals. [20]

The simplest method is hydrolysis. Reaction between precursors in aqueous solution leads to formation and precipitation of cerium (III) hydroxide, which is unstable and immediately transforms into cerium dioxide with oxidation usually by oxygen dissolved in water. Synthesis is usually done at room temperature. Precursors are usually soluble cerium(III) salts and a base such as aqueous ammonia solution, ammonium carbonate or hexamethylenetetramine [21]. Since hydrolysis is the most widely used method, there are many variants with different precursors and particle sizes. These methods are also used to synthesize nanowires instead of isotropic particles [22].

In hydrothermal method, precursors are dissolved in water and the reaction takes place in an autoclave and temperatures higher than 100^{o}C. With elevated temperature and pressure, cerium oxide starts crystallizing out of the solution. This was one of the first times using cerium chloride hexahydrate, citric acid and ammonia water. Using citric acid as stabilizers the particle size was about 5 nm. Without citric acid it was between 100 nm and 200 nm [23]. Most often used precursors are cerium nitrate with stabilizers like citric acid or polyvinyl pyrrolidone. Using hydrothermal methods, it is possible to get nanoceria with specific morphologies like polyhedrons, nanocubes and nanorods. The resulting particles have high uniformity and sizes at the smallest can be around 2-3 nm (Fig. 3).

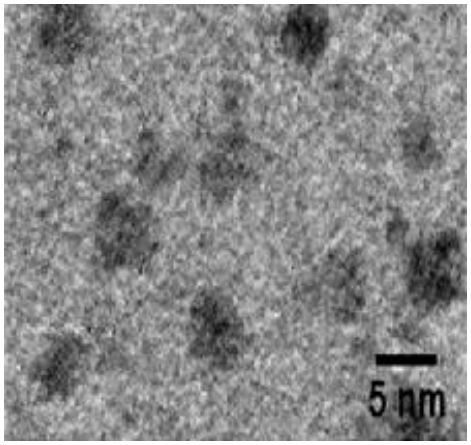

Figure 3. TEM of CeO_2 [24].

Green synthesis methods are becoming more popular to reduce harm to the environment and make sure the particles aren't coated with anything toxic to human cells. These methods are usually easier and safer. These are mostly done at room temperature and atmospheric pressure. The main approaches are nutrient-, plant-, fungus- and polymer-mediated synthesis [25]. Nanoceria was synthesized using aqueous fruit extracts from plant *H. thebaica* and cerium nitrate. The particles were found to be antimicrobial, have antioxidant properties, protein kinase inhibition and potential antiviral properties [26]. In general, green methods are capable of achieving highly uniform particles in different size ranges.

Cerium particles can also be synthesized by general oxidation, sonochemical methods, microwaves, self-propagating high-temperature synthesis. Oxidation methods are where cerium precursor is oxidized by any suitable oxidizer, such as hydrogen peroxide. Increasing the oxidizer concentration led to a decrease in particle size of synthesized particles [27].

Besides the differing oxidation states, cerium particles have other properties that influence biological effects on living cells. In a colloid solution, properties of CeO_2 nanoparticles like surface charge, particle size, and others may have a large role. Aggregation affects the toxicity of CeO_2 nanoparticles in different marine organisms. This happens because of photocatalysis in the presence of ceria aggregates destroying algae lipid layers [28], [29]. Other factor could be dissolution of ceria and emitting of ions into the solutions, but this has been found to be negligible in biological mediums

[30]. The toxicity of ceria nanoparticles seems to be more from contact of particles with cells instead of from internalization. For internalized nanoceria the damage is related to lysosomes and oxidative stress [31]. The mechanism of non-internalized nanoceria toxicity is uncertain. It seems to not be related to shape, concentration, surface charge or nominal size. The effect might be produced by Ce^{3+} on the surface of particles. When surface Ce^{3+} were blocked by phosphate groups, then toxic effects to tested cells disappeared. Growth of cells increased and ROS levels decreased [32].

The first antibacterial properties of cerium compounds were systematically analyzed in 1947. Cerium nitrate was found to be antibacterial, but dependent on the pH of the solution. It was found to be most effective at slightly acidic solutions. [33] Cerium in solutions readily binds to proteins and phosphate groups, leading to precipitation in solution and reducing concentration of available cerium [34]. Cerium has been shown to be non-toxic to mammalian cells, but has been shown to be cytotoxic to cancer cells. [35]. Different mechanisms of toxicity have been proposed. In many cases the main mechanisms have been thought to be oxidative stress or related to cerium oxide's catalytic activity. These and similar nanoparticles are called nanozymes, because they have similar properties to enzymes [36]. This seems unlikely, because in biological applications nanoceria typically acts as an antioxidant, while it catalyzes mostly oxidation processes [37]. A way to measure antioxidant properties is by measuring hydrogen peroxide and hydroxyl radical concentration in water after X-ray radiation [38].

The exact biological effect of ceria and silver nanoparticles is not yet fully understood. Because of this different methods or study are of great interest, but bio-objects are complex and difficult to prepare and analyze. Because of this, it is often more informative to use simpler molecules that make up larger biomolecules as models to study the effects of different nanoparticles. In this work several amino acids and Bovine Serum Albumin (BSA) protein were studied before and after treatment with synthesized nanoparticles using spectroscopic methods briefly described below.

1.3. Spectroscopical analysis of amino acids and proteins and their interaction with nanoparticles

1.3.1. Infrared spectroscopy

IR spectroscopy is a type of spectroscopy using absorption of infrared light for structural analysis of materials. It is one of the most common methods to analyze structures of small molecules, because of its high sensitivity to chemical composition and structure. IR spectroscopy is one of the most widely used methods to analyze proteins and other biological materials.

Absorption of infrared light excites the vibrational transitions of molecules. This generally happens when the frequencies of light and vibrations are equal and molecular dipole moment changes during the vibration. The vibrational frequencies are affected by molecule structure and because of this affect the positions of absorption bands in IR spectroscopy. The positions of absorption bands are approximately determined by vibrating masses and the type of bond, either single, double or others. The absorption bands are more exactly determined by electrons being withdrawn and donated because of intra- and intermolecular effects and different vibrations overlapping. All polar bonds in the molecule contribute to the absorption spectra. This can be a problem with larger molecules. The studied bands can be easily overlapped by broader inconsequential absorption bands [39].

The main information that can be obtained from the infrared spectrum is from the chemical structure of the vibrating group. It is the dominating effect that determines vibrational frequencies because of the strength of the vibrating bond and mass of the vibrating atoms. While the exact chemical structure is often hard to determine because of overlapping bands, changes in chemical structure can be detected. These are generally changes, such as forming a new chemical bond [40]. Other changes that can be seen include chemical reactions catalyzed by enzymes [41]. Other information that can be obtained are chemical properties of neighboring groups of molecules, redox states, bond angles, conformational freedom, hydrogen bonding and electric fields.

The two most common geometries used in IR spectroscopy are FTIR and FTIR-ATR. FTIR uses IR source guided through a solution in a cuvette to measure absorption in the

sample. The cuvette used for samples cannot have an effect on the IR beam, commonly quartz cuvettes. The other method is attenuated total reflectance, which uses a crystal. ATR avoids the need for additional sample preparation by having the sample be placed directly on the ATR crystal. The crystal needs to have a larger refractive index than the sample, and is usually larger than 2. One common ATR crystal is diamonds. Infrared light is directed into the crystal at an angle of incidence that results in total reflection at the interface of sample and crystal (Fig. 4). Upon reflection some light penetrates into the sample and is absorbed. The light reaching the detector carries information about the samples IR spectrum.

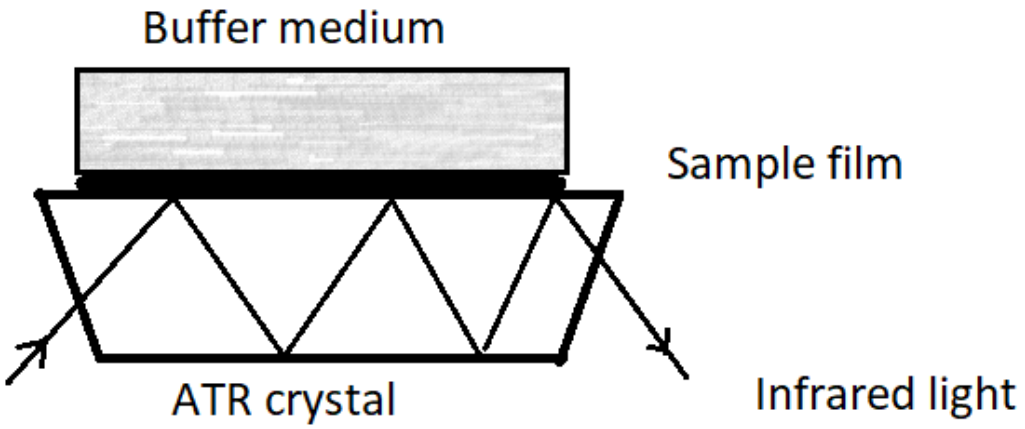

Figure 4. Typical ATR setup.

When measuring proteins, a film is usually formed by dropping protein solution on the crystal and waiting for it to dry. Since some proteins can have differing properties in dry conditions, a buffer of water or other solvent can also be added.

1.3.2. Luminescence and CD spectroscopy

Other methods allowing to see structural changes in proteins or amino acids include luminescence and Circular Dichroism (CD) spectroscopy. Luminescence spectroscopy works on the principle of luminescence, which happens when electrons in a compound get excited and thermal relaxation is hindered. This causes the compound to emit photons to achieve a state of minimal energy. When there are changes to the electron structure of

the compound, there will also be changes to the luminescence spectra of the compound. Proteins are often luminescent because of the amino acids, that proteins are made of. One such amino acid is tryptophan. Tryptophan has intrinsic luminescence because of its indole side chain, which has a delocalized electron structure.

The most common methods of measuring luminescence intensity are measuring the samples intrinsic luminescence. There are derivatization methods in which non-luminescent analyte is changed to a luminescent derivative and quenching methods in which the sample is changed to quench luminescence and the reduction in the intensity of luminescence is analyzed. It is possible to interpret changes to the sample molecules from changes in the luminescence intensity and shifts in the wavelength of the peak maximum, but it is complicated in the case of complex molecules, which is why often only tryptophan luminescence is measured in proteins.

Tryptophan luminescence is particularly suited as a tool to study proteins in solution as its emission maximum is a sensitive indicator of the local structure and polarity in the environment surrounding the side chain of the amino acid. As an example, the emission maximum of tryptophan shifts to the red, when its side chain is exposed to hydrophilic environments [42].

Circular dichroism is an absorption spectroscopy method, that is based on differential absorption of left and right circularly polarized light. Optically active chiral molecules will absorb one certain direction of polarized light. The differences between these two types of polarized light can be measured and quantified. One of the most widely used application of circular dichroism is identifying protein structures. The information from the circular dichroism of proteins is primarily the absorption of the amide chromophore and the results expressed as molar ellipticity. This chromophore starts absorbing light in the UV region, with the first band appearing at about 220 nm [43]. The ellipticity of the protein depends on secondary structure of the protein. The typical structures for which characteristic spectra exists are α-helix, β-sheet, β-turn and random coil, (Fig. 5). Circular dichroism can be used to measure changes in protein secondary structures. Some information can also be obtained about tertiary structure of proteins. Absorption in near-UV region is due to dipole orientation and surrounding environment of the amino acids.

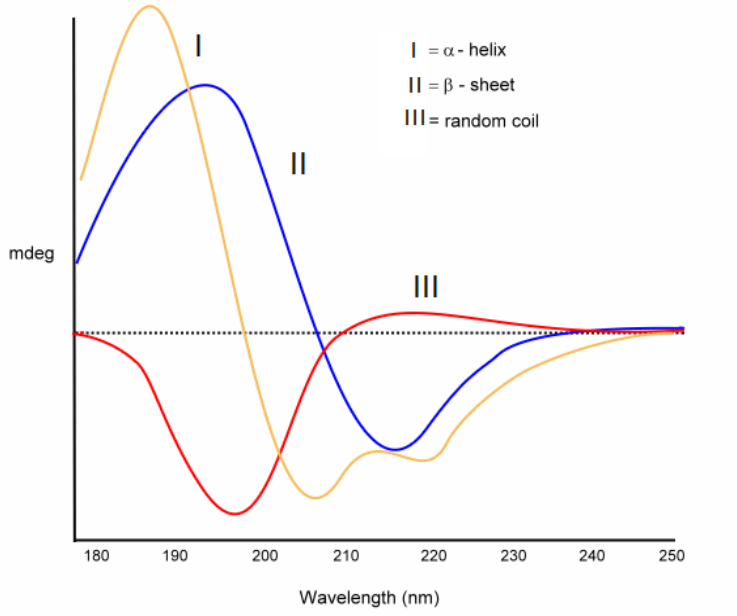

Figure 5. Protein secondary structures, graph modified from [44].

2. Experimental

2.1. Silver nanoparticles synthesis

Silver was synthesized in two different methods. Materials used for synthesizing silver particles were $AgNO_3$ 0,1M aqueous solution, $CitNa_3$ 99% pure from Sigma-Aldrich, 10000 molecular weight poly(vinylpyrrolidone) (PVP), $NaBH_4$ 98% pure from Sigma-Aldrich. All solutions are made with de-ionized water. First method used was Turkevich [7] method for gold particle synthesis modified for silver nanoparticles. First step is to form an aqueous solution of sodium citrate, by adding 0.29 g of sodium citrate to 500 mL of water to make around 0,002M solution and heated up to around 90°C. After this 2.5 mL of 0.1M $AgNO_3$ was added with vigorous stirring. The ongoing reaction is shown on Fig. 6. The solution was left to stir for around 1 hour, until the solution turned from transparent to opalescent yellow, signaling the formation of a colloid solution. Next steps were to centrifuge the solutions at 10000 RPM or 11600 G at 1-2 hours using Heraeus Multifuge X1 centrifuge, depending on the amount of citrate used to stabilize the solution. In several cases, it was impossible to separate nanoparticles by centrifugation of reaction solution. To reduce the stability of the colloid we added 0.3 wt.% of $NaNO_3$ to the solution in order to increase its ionic strength. After that it was possible to use the centrifuge to separate out the particles. The precipitate was collected and redissolved into a more concentrated solution. After multiple redispersion and reprecipitations the solution was ultrasonicated until formation of clear colloidal solution. In case of silver the resulting colloid looked red-orange.

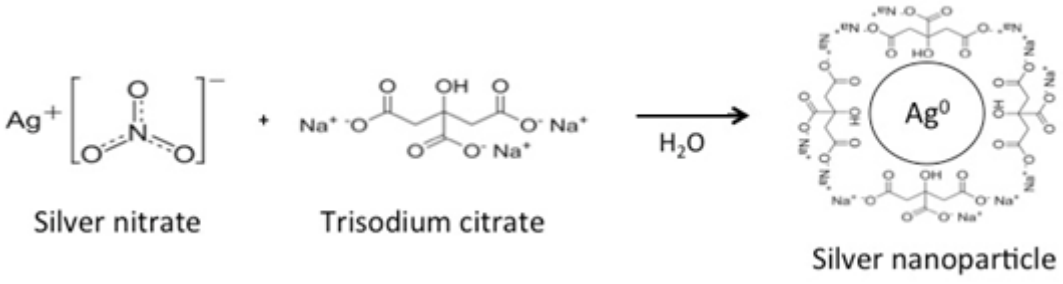

Figure 6. Synthesis and capping of silver particles.

The second method is a modified synthesis originally used to make silver nanoprisms at room temperature [45]. This method uses $NaBH_4$ and silver nitrate solution with PVP to

prepare a small amount of silver particles in an aqueous solution to aid in the nucleation, which will be called the seed solution. The seed solution was made by first preparing 5 mL of 2.5 mM aqueous solution of trisodium citrate. Then 0.25 mL of 10000MW PVP with a concentration of 0.5 g per 100 mL was made and added to the trisodium citrate solution. Next 0.3 mL of 10 mM freshly prepared solution of $NaBH_4$ is added to the solution. Then 5 mL of 0.5 mM $AgNO_3$ is added slowly while mixing to form the seed solution. The flow rate should be around less than 2 mL per minute or one droplet from the burette at a time, to ensure proper mixing. 27 mL of the prepared seed solution was added to 472 mL of 4.6 mM solution of sodium citrate to a total of 500 mL and heated to around 90^{o}C. Then 0.625 mL of 0.1M $AgNO_3$ was added and stirred vigorously for around 30 minutes until yellow opalescent color appeared. The centrifugation and washing were similar to the first method.

2.2. Ceria nanoparticles synthesis

The materials used for cerium synthesis were as follows. Cerium (III) nitrate hexahydrate, 99% purity, obtained from Sigma-Aldrich, analytical grade hexamethylenetetramine from Sigma-Aldrich, diammonium cerium (IV) nitrate 98% purity from Fluka analytical, citric acid 99% purity from Fluka analytical, 30% aqueous ammonia solution. All solutions were made with de-ionized water. Cerium was synthesized in two different methods. First method was modified from [46]. It is a hydrolysis reaction between ceric ammonium nitrate and hexamethylenetetramine and results in ceria particles, ammonia and formaldehyde (Eq. 1).

$$(NH_4)_2(Ce(NO_3)_6) + (CH_2)_6N_4 + H_2O \rightarrow CeO_2 \downarrow + NH_3\uparrow + CH_2O\uparrow \quad (1)$$

The solution is prepared from diammonium cerium (IV) nitrate and HMTA. 0.189 g of $(NH_4)_2Ce(NO_3)_6$ and 0.053 g of HMTA were added together into an autoclave vessel. Around 50 mL of water is added, so that around half of the autoclave vessel is filled. The vessel is sealed and heated to 180^{o}C for 30 minutes. After thermal treatment, the vessel is cooled down in a water bath. The product is centrifuged for 5 minutes, the sediment washed with de-ionized water and redispersed. These steps are repeated 3 times and final product redispersed as a more concentrated solution. The final solution is ultrasonicated and the solution should look pale yellow.

The second method was modified from [38]. The reaction is a two-step process. First is a hydrolysis reaction. Second step is oxidation where the product immediately decomposes into ceria (Eq. 2).

$$Ce(NO_3)_3 + NH_4OH \rightarrow Ce(OH)_3 + NH_4NO_3 \rightarrow Ce(OH)_3 + O_{2(aq.)} \rightarrow CeO_2\downarrow + H_2O \quad (2)$$

Ceria nanoparticles were prepared by first dissolving 0.045 g citric acid in 25 mL of a 0.05 M aqueous solution of cerium (III) nitrate. The solution is rapidly added into a 100 mL 3M solution of ammonia and left to stir vigorously for 2 hours. After the addition of cerium solution, the solution changes color from transparent to yellow-orange. After the synthesis the colloid solution is centrifuged, washed and concentrated. The first centrifugation is done at 10000 RPM for 30 minutes. The supernatant is clear and can be poured off completely, the particles are washed, redispersed and centrifuged again for 10 minutes. This step is repeated until there is no more scent of ammonia. The final solution is redispersed, sonicated with ultrasound and looks dark yellow.

For distribution of synthesized nanoparticles on the surface of porous materials and feathers two methods were used: 1) Submerging the material on the colloid solution for around 15 minutes with subsequent drying at room temperature. 2) Using of air-propelled paint-spray gun to pulverize the colloid. In this case the processing was done for a period needed for all the volume of the treated sample to become visually dump. Again, with subsequent drying at room temperature.

2.3. Methods of analysis.

Particle size and morphology were studied by means of electronic microscopy. SEM device used was Nova NanoSEM 450, TEM device was FEI Titan Themis 200 Cs-corrected TEM. DLS and Zeta potential measurements were done with Malvern Zetasizer Nano ZSP, UV-Vis with Agilent Cary 5000 UV-Vis-NIR Spectrophotometer. The measurement range for UV-Vis was from 800 nm to 250 nm.

CD was done with Chirascan Plus spectrophotometer (Applied Photophysics, UK), spectral range 180-1100 nm, spectral resolution 0.5-4 nm. For CD measurements, all the

samples were preliminary to achieve an optical density of less than 0,8. Ceria colloids were finally diluted approximately 50 times.

IR measurements were obtained with Bruker Vertex 70 spectrometer. Measurements were done in ATR configuration and the ATR crystal was a diamond. Detector used was a mercury cadmium telluride or MCT detector. Data was obtained from the range of 4000 cm^{-1} to 400 cm^{-1}. The settings used for IR measurements were the following: resolution 2 cm^{-1}, sample scan time 120 scans, background scan time 120 scans, aperture width was 1 mm and scanner velocity 10 kHz.

The measured protein was BSA, bovine serum albumin (Cell culture grade, 10% solution in PBS). Amino acids were tryptophan (powder, Reagent grade), histidine (powder, Reagent grade), alanine (powder, Reagent grade). The samples were mixed together in 1 to 1 ratio with different synthesized nanoparticles and protein or amino acid, leaving them to react for 15 minutes, and then centrifuged for 10 minutes at 15000 x g before measuring the IR spectra. The samples were prepared for IR measurements by adding droplets onto the ATR crystal and dried with a blow drier. Around 1 microliter of water was added to act as a buffer.

Luminescence measurements were carried out with Horiba Fluoromax-4 spectrophotometer. Signal integration time was 0.5 s, slits width was 1 nm. The samples were prepared by mixing amino acids with particles, leaving them to react for 15 minutes, centrifuged for 10 minutes and then the liquid sample was used as the sample for measurements. The samples were added to a quartz cuvette. We used a UV filter for excitation slit in order to cut off the second harmonics in the excitation beam.

3. Results and discussion

3.1. Nanoparticle morphology

Results of microscopy for the citrate-reduced and seed-mediated silver nanoparticles are presented below. Citrate method has a strong advantage for its simplicity and scalability, which is very important from the point of view of future applications. However, from the SEM images (Fig. 7) one can see that particle distribution was more even and the mean size smaller for the seed-mediated synthesis method. Citrate-reduced silver particles mean size from SEM was ~ 30 nm. For seed-mediated particles, we did also TEM imaging (Fig. 8) and determined the mean particle size to be around 15 nm. The size distribution was also characterized by DLS method. For citrate-based particles the measured mean hydrodynamic size was around 40 nm and for the seed-mediated particles it was 18,5 nm, which is in good correlation with microscopy data.

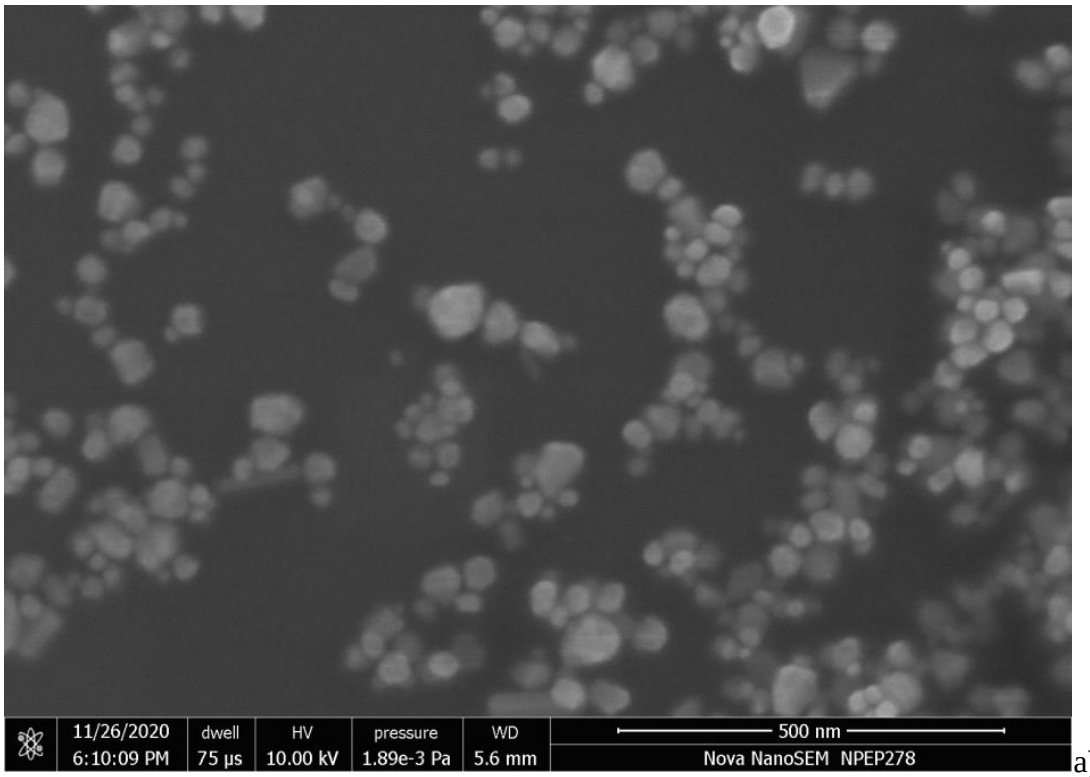

a)

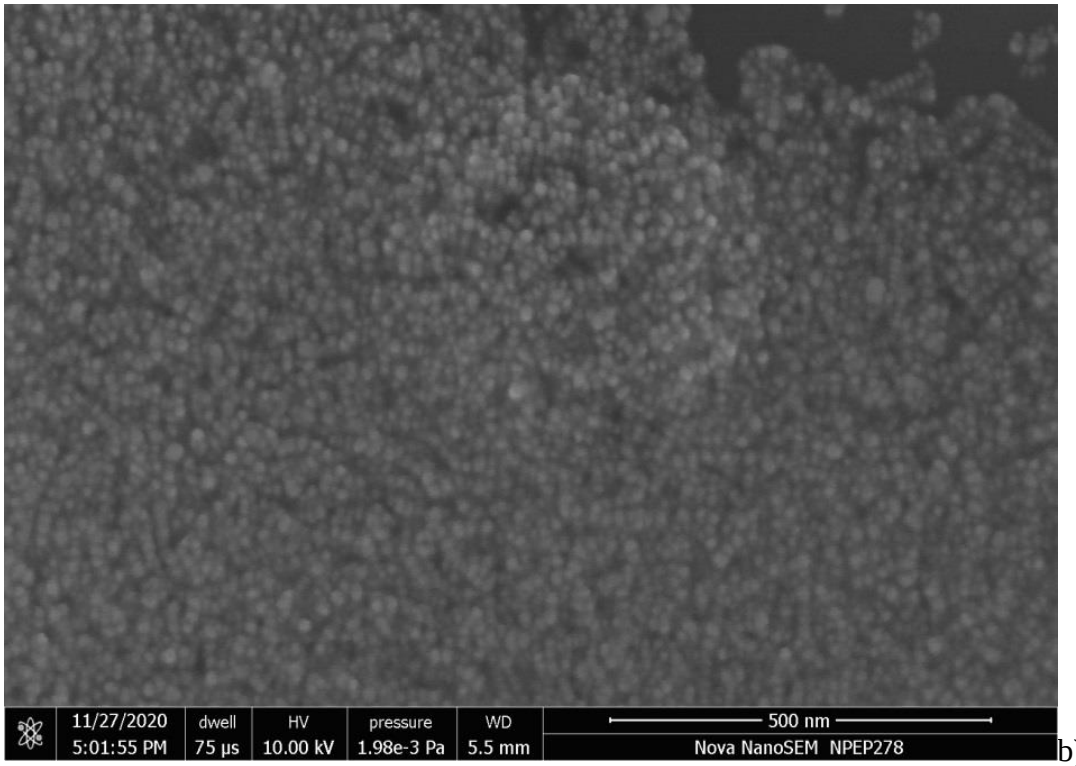

b)

Figure 7. SEM images of a) citrate-reduced silver particles. b) seed-mediated silver particles.

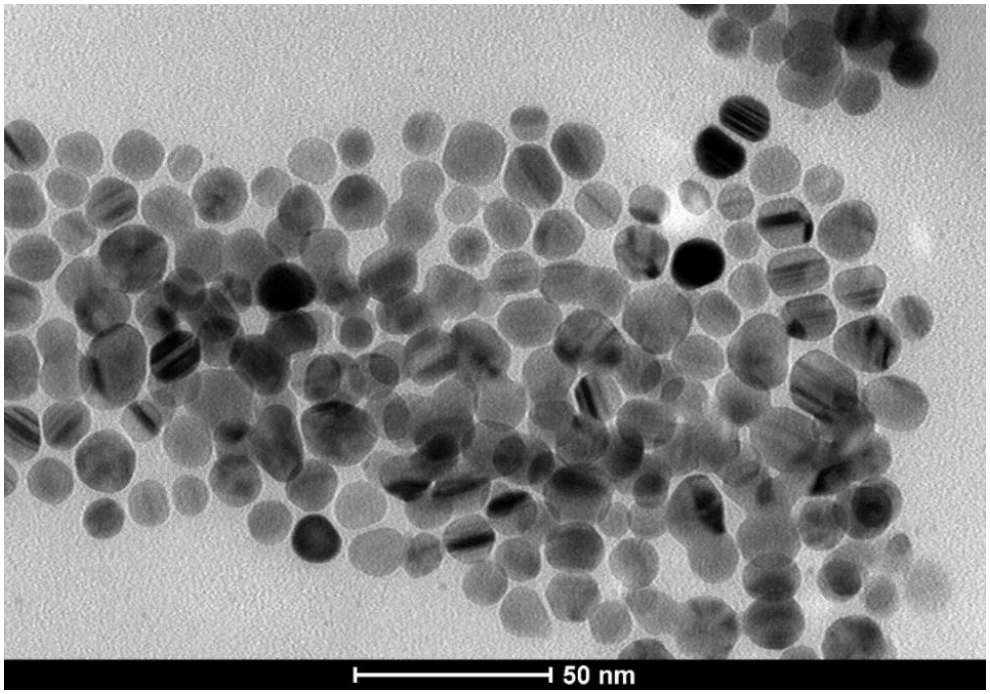

Figure 8. TEM of seed-mediated silver particles.

The UV-Vis shows absorption maximum for the surface plasmon resonance (Fig. 9) at 426 nm for citrate-route and 405 nm for seed-mediated Ag nanoparticles, also correlating with electron microscopy and DLS data. One can notice wider absorption band for citrate-reduced nanoparticles, which is due to wider size distribution. In addition, we measured the zeta-potential of our silver particles, which was around -52 mV for seed-mediated nanoparticles (for citrate-route nanoparticles the size distribution appeared to be too wide to obtain conclusive results of DLS measurements), which illustrates high stability of silver nanoparticles in water colloids. Because of these results we decided to continue our further experiments concerning functional properties of synthesized nanoparticles with only the seed-mediated synthesis method.

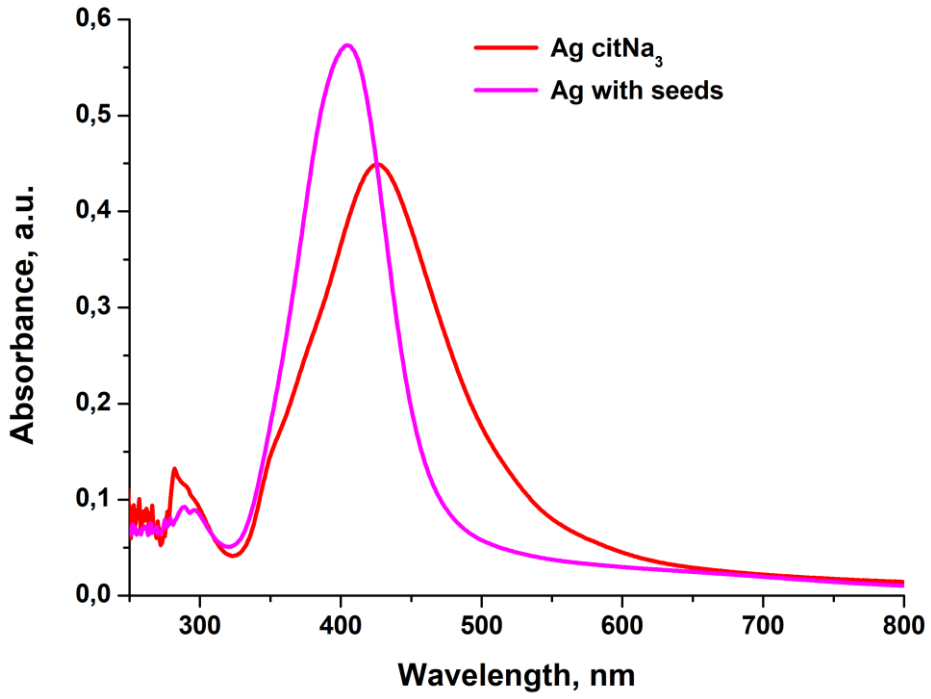

Figure 9. UV-Vis of silver particles.

In the case of CeO_2 nanoparticles synthesis, both methods allowed to obtain quite stable in aqueous colloids nanoparticles with uniform shape and narrow size distribution.

However, functional properties of synthesized nanoparticles appeared to be quite different in many cases and will be discussed in comparison. From this point on they will be referred to as positively charged (HTMW route) and negatively charged ceria particles (precipitation route) due to the surface charge of synthesized nanoparticles, which will be discussed further in this section.

Cerium particles were too small for SEM for a representative image of the particles. From the TEM images (Fig. 10) the mean particle size of both CeO_2 estimated as around or a bit less than 5 nm.

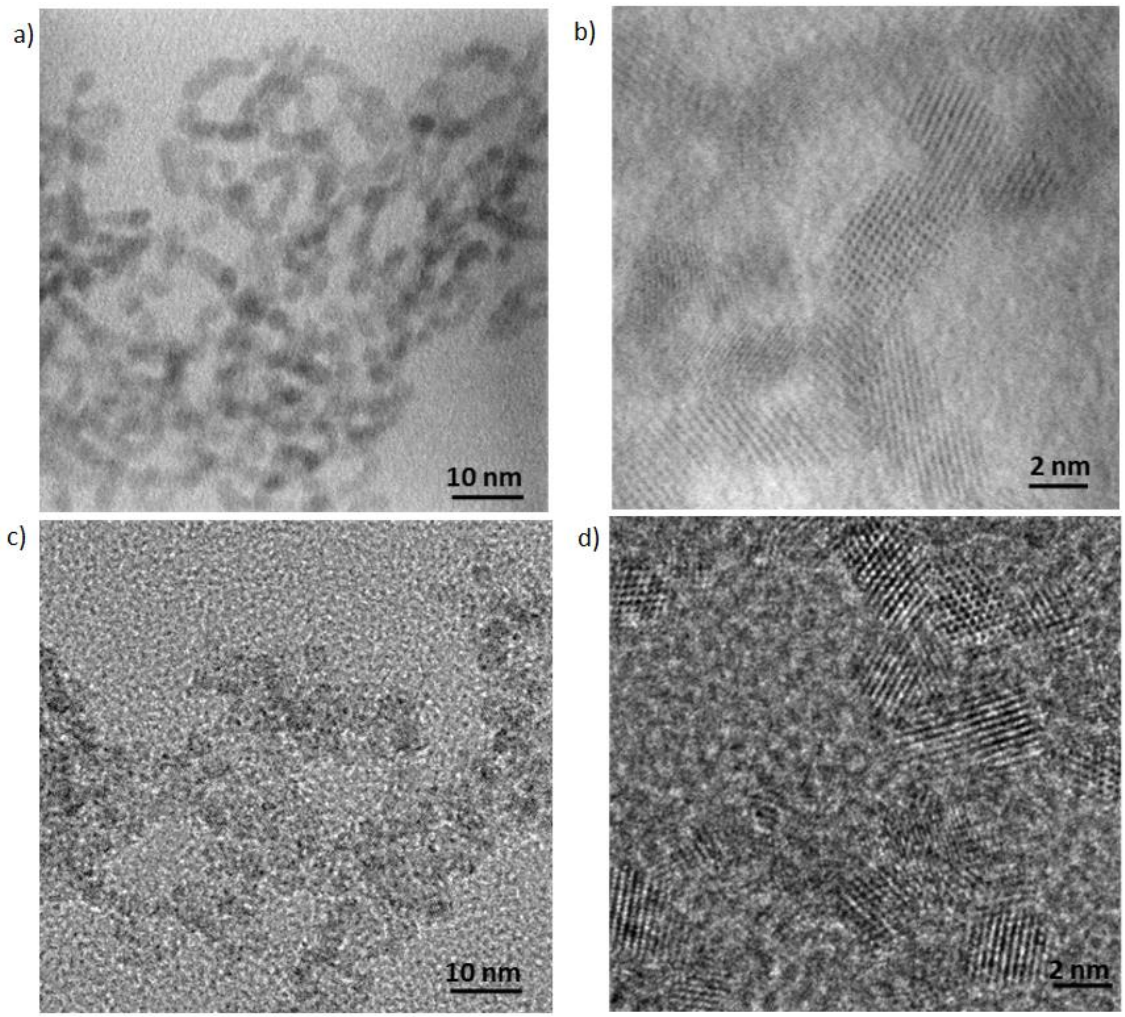

Figure 10. TEM images of positive ceria particles a), b) and negative ceria particles c), d).

The designations “negative” and “positive” for synthesized samples come from the results of the zeta-potential measurements, as for sample synthesized using HTMW method the measured z-potential was +41 mV and for the nanoparticles synthesized by precipitation it was around -53 mV. Positive and negative ceria particles have similar sizes in DLS, being around 7 nm (positive) and 4.5 nm (negative) (Fig. 11), which does coincide with the TEM measurements. Also DLS measurements show wider peaks for larger sizes, corresponding to the aggregates, containing various amount of individual particles.

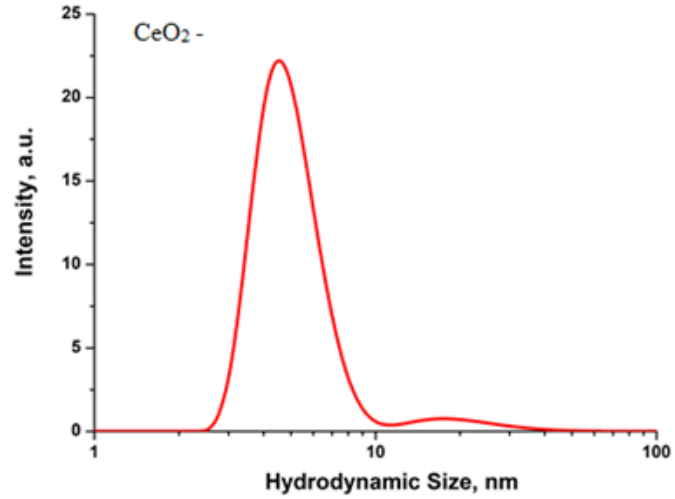

a)

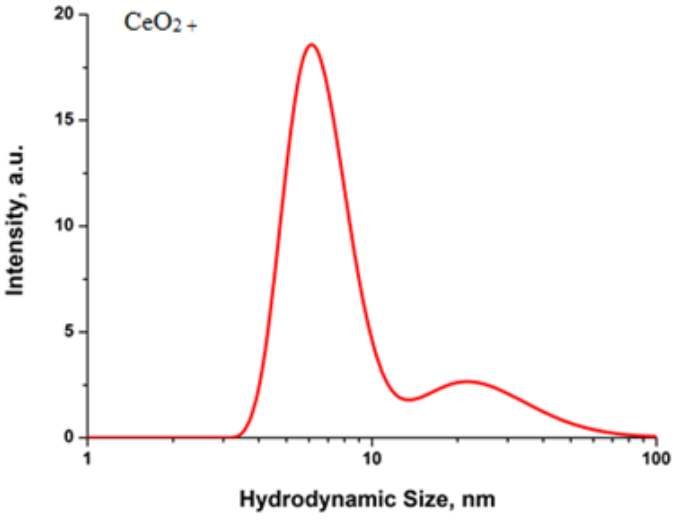

b)

Figure 11. DLS of a) negatively charged particles b) positively charged particles.

UV-Vis spectroscopy was also performed for CeO_2 nanoparticles. It was shown, that fundamental absorption edge is blue shifted (approximately 10 nm) for positively-charged

CeO_2 nanoparticles (Fig. 12). This shows that the synthesis methods resulted in particles with different properties, probably the oxidation state of cerium atoms on the surface. It is in good correlation with visual observation of colloids, as the negative CeO_2 particles look a lot darker yellow compared to the positive CeO_2. However, the darker color might also originate from oxidized and polymerized citrate ions on the surface of the particles.

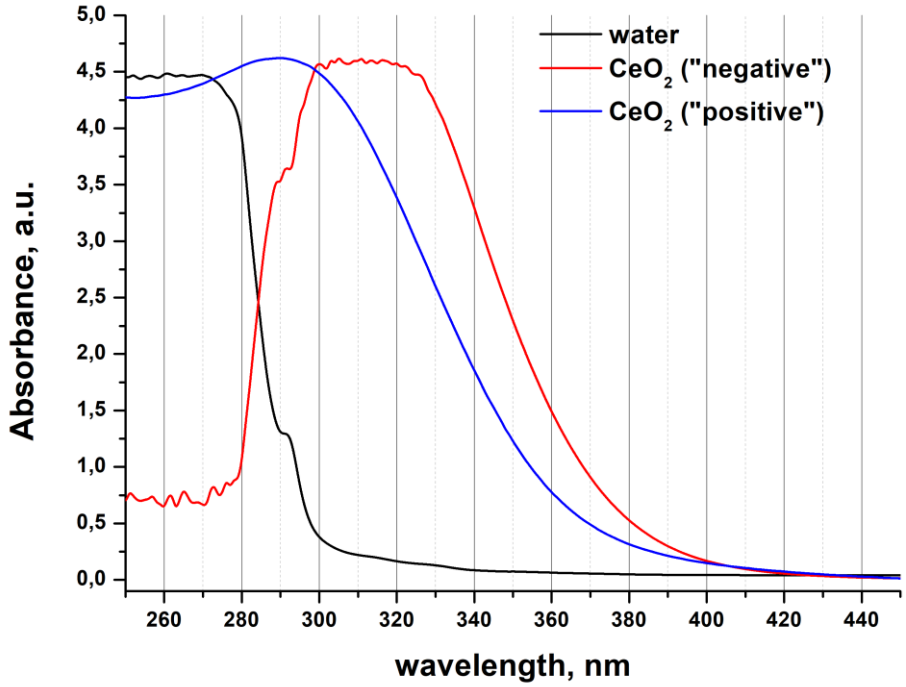

Figure 12. UV-Vis spectra of two types of nanoceria.

Synthesized CeO_2 particles were also studied with IR spectroscopy (Fig. 13). Experimental CeO_2 IR spectrum is quite in agreement with the literature data [47] and exhibits peaks in around 3600 to 3200 cm^{-1}, which corresponds to -OH stretching of absorbed water and surface OH-groups. Peaks around 1600 cm^{-1} and 1400 cm^{-1}, which are H-O-H deformational vibrations and C-O stretching vibrations from surface water molecules and carbonate ions, respectively. The peak from 800 to 500 cm^{-1} is due to Ce-O stretching vibration.

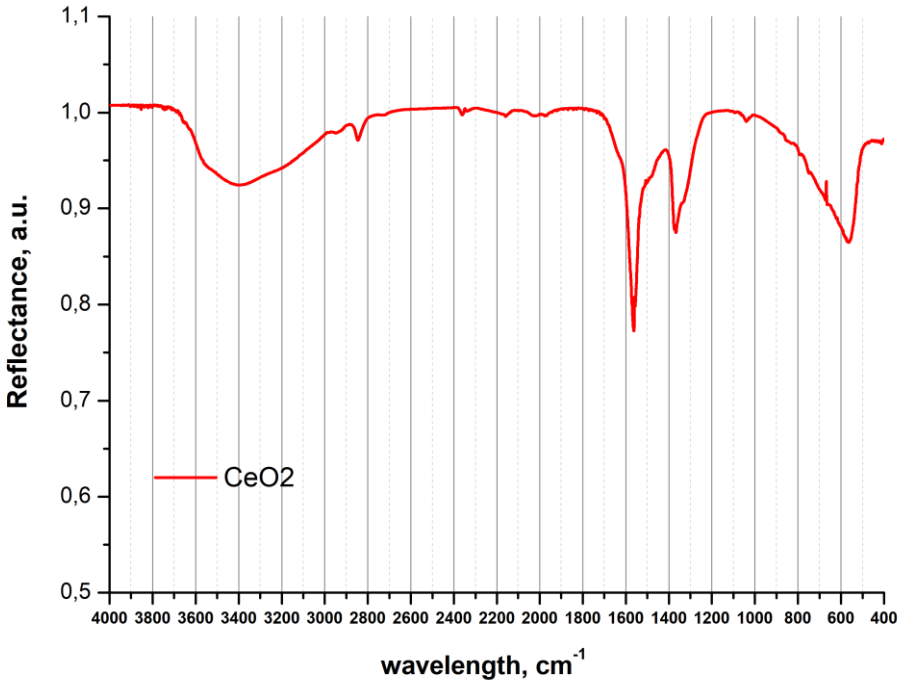

Figure 13. IR spectra of CeO_2.

3.2. Distribution of synthesized nanoparticles on the surfaces

In order to understand the applicability of synthesized colloids for future application as antiviral treatment agents, we tried distributing silver and CeO_2 nanoparticles onto various soft surfaces, including polymeric fabrics used for linen, porous polymeric foams and bird feathers, used as mattress and cushion fillers, respectively. Unfortunately, in most cases after treatment we were unable to microscopically detect the presence and distribution of any particles on the fabric, as the size of the synthesized nanoparticles was smaller or comparable with the size of the surface roughness or debris on the material (see Fig. 14 for comparison of polymer fabrics before and after application of silver nanoparticles).

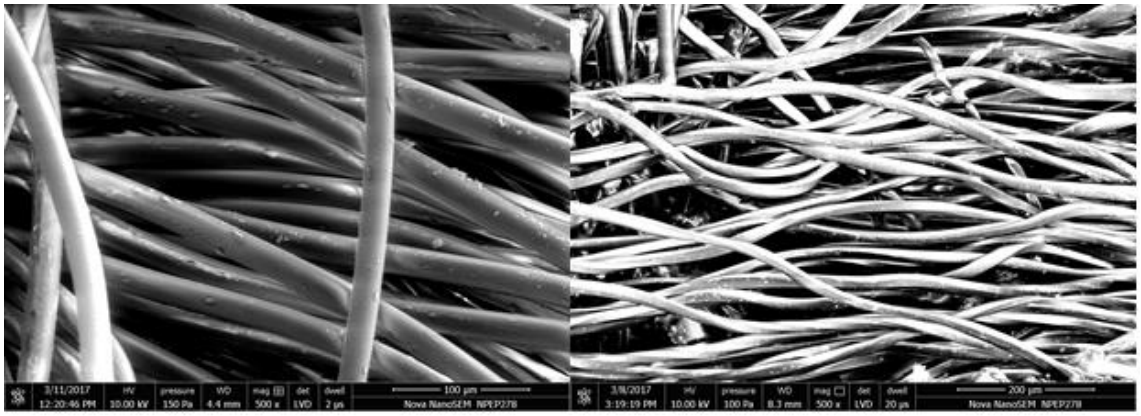

Figure 14. SEM of fabrics, untreated on the left, treated with Ag nanoparticles on the right.

However, we were successful in studying the distribution of silver nanoparticles on the feathers used as fillers for cushions (Fig. 15). This was achieved by submerging the material into the colloid solution for around half an hour and then washing it with water. One can see, that nanoparticles are uniformly distributed on the feathers surface as individual or aggregates of 2-5 nanoparticles.

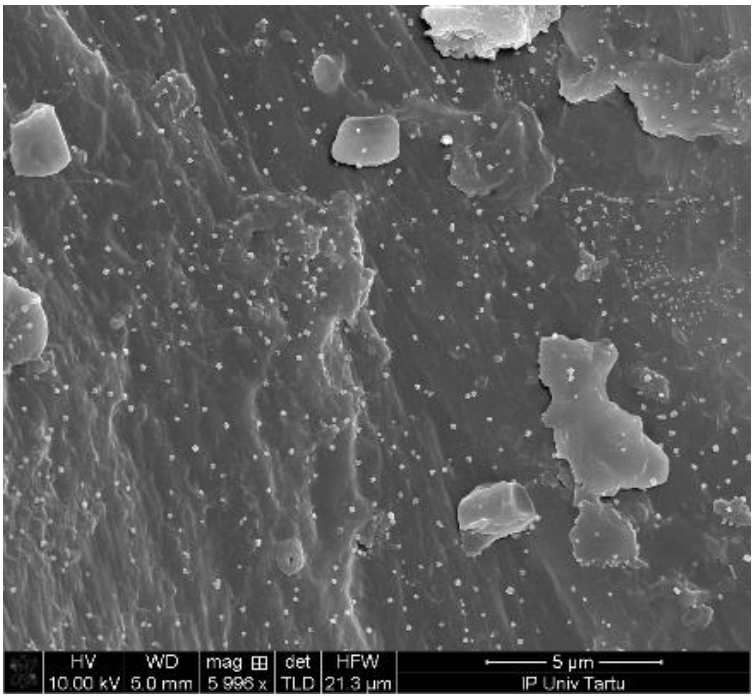

Figure 15. SEM of porous biological material.

3.3. Study of the effect of synthesized nanoparticles on model amino acids and BSA protein.

3.3.1. IR and luminescent spectroscopy of amino acids after treatment with synthesized nanoparticles

We studied IR spectra and luminescence behavior of several amino acids in water solution after treatment with colloids of synthesized nanoparticles. Water solutions of corresponding amino acids were mixed with aqueous colloids of nanoparticles, stirred for a certain time and afterwards nanoparticles were removed by centrifugation to avoid them affecting the spectral measurements. As model examples of amino acids, we chose tryptophan (hydrophobic luminescent side-group), histidine (hydrophilic luminescent side-group) and alanine (CH_3–, non-luminescent side-group). Alanine was chosen as one of the simplest amino acids in order to understand the influence of synthesized nanoparticles on the main functional groups of amino acids. Tryptophan and histidine are exhibiting luminescence, which is known to be very sensitive to any structural changes and therefore can provide valuable information. Tryptophan and histidine samples were studied by means of both IR and luminescence spectroscopy. Alanine does not exhibit luminescence and therefore was studied only by means of IR spectroscopy.

As the first attempt to understand the influence of synthesized nanoparticles on the structure and properties of amino acids we conducted series of measurements of IR spectra of alanine (Fig. 16) untreated and treated with nanoparticles (Fig. 17).

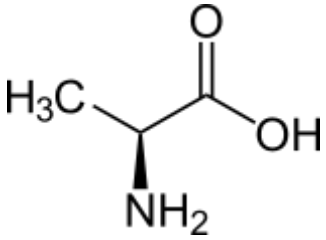

Figure 16. Structure of an L-alanine molecule.

Alanine allows to study the effects of nanoparticles on the main functional groups of amino acids, namely amino-group carboxyl group. Obtained result showed that nanoparticles have minimal effect on these groups.

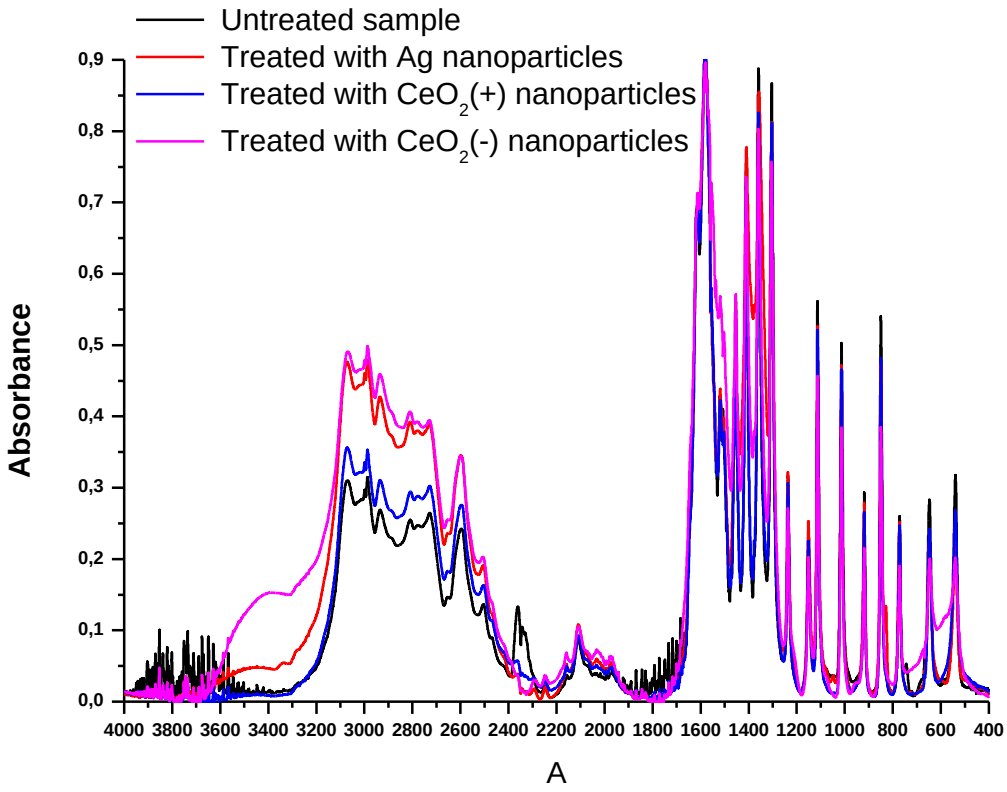

Figure 17. IR spectra of untreated alanine and alanine treated with synthesized nanoparticles.

Both positively and negatively charged nanoparticles of CeO_2 seem to have no effect on alanine structure, according to IR (broad bands around 3400 cm^{-1} appear from not fully dried solvent, water, while medium strength bands around 2350 cm^{-1} on the spectrum of untreated alanine is undercompensated lines of CO_2 from atmosphere). Treatment with silver nanoparticles leads to slight changes (red shifts of 850 cm^{-1}, 1359 cm^{-1} and 1411 cm^{-1} bands and appearance of new 828 cm^{-1} band) (Fig. 18).

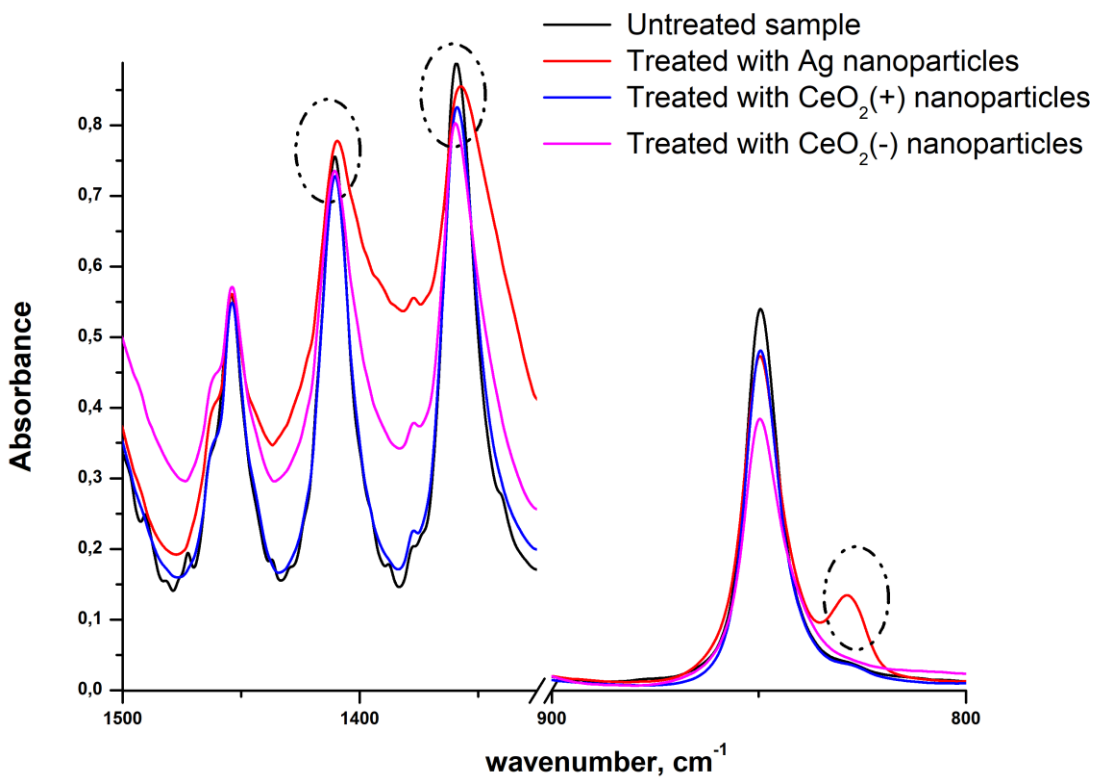

Figure 18. Enlarged part of IR spectra of untreated alanine and alanine treated with synthesized nanoparticles. The middle of the spectra was cut out to increase the visibility, bands are practically identical for all samples in the omitted region.

All these bands are associated with carboxyl group [48], [49] and the red shift indicates most likely formation of a salt with Ag^+ ions, which are forming in the colloidal solution of silver nanoparticles due to their partial dissolving. Further it will be shown, that in case of other amino acids silver nanoparticles exhibit similar effect. In case of cerium dioxide nanoparticles analogous effect is not observed probably due to their extremely low solubility.

Tryptophan (Fig. 19) is an amino acid with indole as a side-chain group. It is considered to be a hydrophobic side-group, which manifests in relatively poor solubility of this amino acid in water.

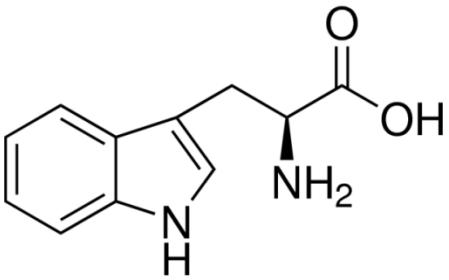

Figure 19. Structure of an L-tryptophan molecule.

Indole group is also responsible for luminescent properties of this compound. Luminescent properties of indole itself, tryptophan and its derivatives have been extensively studied [50]–[55] and therefore it's a good model system to reveal the effect of nanoparticles. On Fig. 20 presented the emission and excitation spectra of tryptophan, untreated and treated with nanoparticles colloids. On the emission spectra one can see (Fig. 20-a), that only treatment of amino acid with colloids of positively charged CeO_2 nanoparticles lead to change in the position of emission bands. We observed significant red shift (around 14 nm for 361 nm band and around 25 nm for 690 nm band, which both correspond to approximately 0.1 eV shift of energy levels).

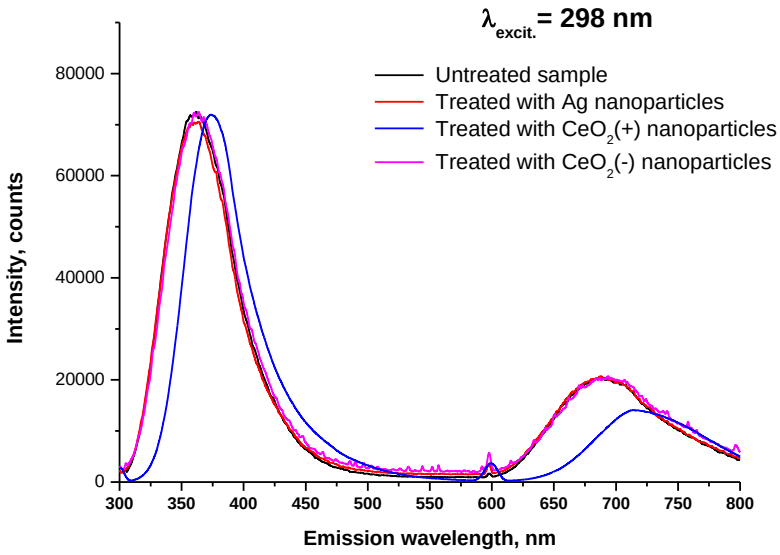

a)

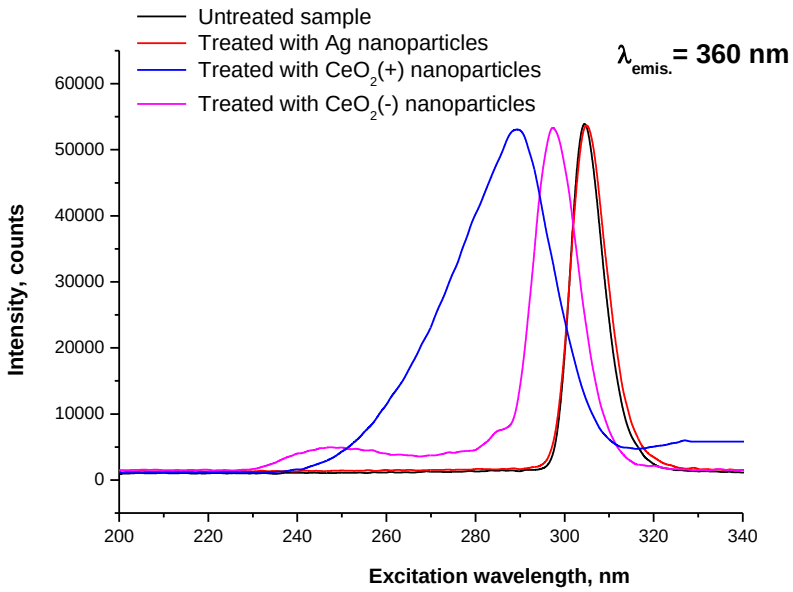

b)

Figure 20. Emission (a) and excitation (b) luminescence spectra of untreated tryptophan and tryptophan treated with synthesized nanoparticles.

The red shift of the indole or tryptophan luminescence is a quite well-known and studied effect [51]. It is usually related to the environment of the indole-group, like polarity of solvent, hydrogen- or charge-transfer bonding. Theoretical calculations [53], [54] shows that among the main excited states of indole (^1L_a and ^1L_b) the former is characterized by much larger dipole moment and therefore is very sensitive to the polarity of the environment. For a free molecule in vacuum, as well as for real solutions in non-polar media, this state is higher than ^1L_b, but in more polar solutions it becomes energetically more favorable (Fig. 21), so the lowest excited state changes and red shift is observed [54].

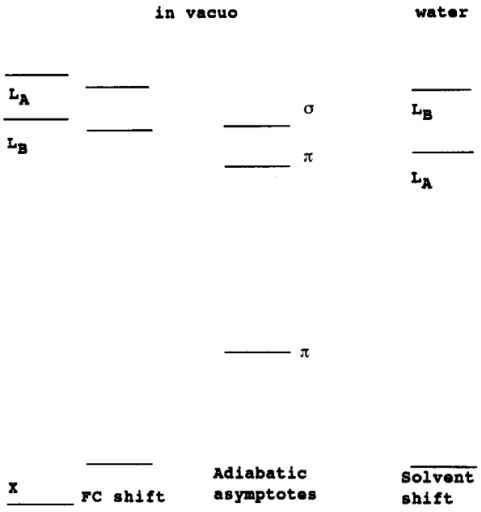

Figure 21. Schematic of ground- and excited-state energies describing the Franck-Condon shift and solvent shift in indole [54].

However, our experimental situation is different, as solvent shift is a reversible effect, which disappears upon the exchange of the solvent of the indole-based compound back to non-polar. Removal of CeO_2 nanoparticles, on the other hand, did not eliminate their effect on the tryptophan luminescence. Thus, there was some structural change, that lead to irreversible shift of the luminescence. This suggestion is indirectly proved by the quantitative comparison of the observed red shift with known literature data [53]. For studied tryptophan-containing proteins in various environments the largest shift led to the maximum of luminescence at ~365 nm, but in our system this maximum shifted as far as 374 nm. This suggests somewhat stronger binding than just a hydrogen bond with the solvent molecules.

On the luminescence excitation spectra (Fig. 20-b) for sample treated with positively charged CeO_2 nanoparticles, the excitation band is blue-shifted by 15 nm. But unlike in emission spectra, a smaller (7 nm), yet still quite visible blue shift appears also for sample treated with negatively charged CeO_2 nanoparticles. Such shifts are also uncharacteristic for a classical solvent shift in tryptophan, as its ground state has very small dipole moment and therefore usually is not sensitive to the environment [54]. However, blue shift of excitation spectra is usual for tryptophan derivatives, such as well-studied N-acetyl tryptophan amide (NATA), see for example [56]. This also indirectly proves that a chemical process occurred in the system after introduction of positively charged CeO_2 nanoparticles. As there were no additives used during treatment of tryptophan and CeO_2

nanoparticles were prepared without any surfactants, which could interact with amino acid, the only possible process could be dimerization of tryptophan. Formation of tryptophan dimers with amino-group of one molecule attaching to the carboxyl group of the other molecule are known, but their formation does not lead to the observed features in the luminescent spectra [55]. Thus, our hypothesis is that CeO_2 nanoparticles selectively catalyze the process of attaching of the NH-group from the pyrrole ring of one tryptophan molecule to the carboxyl group of another molecule of tryptophan.

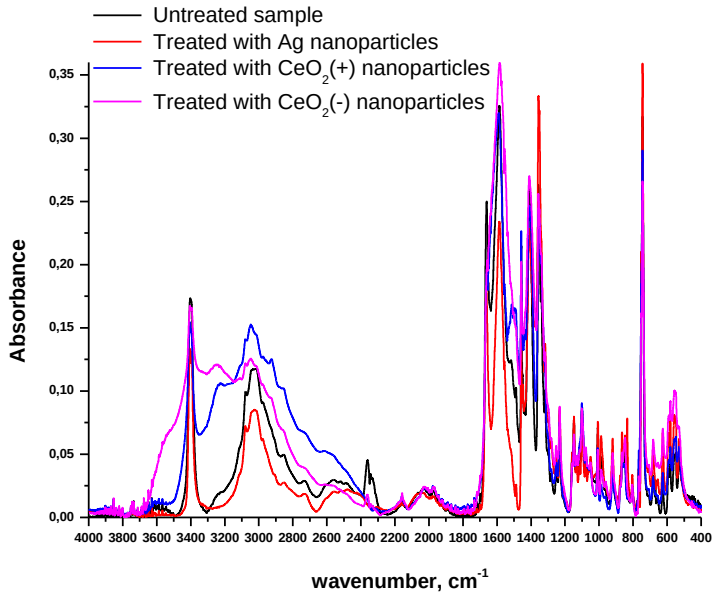

Figure 22. IR spectra of untreated tryptophan and tryptophan treated with synthesized nanoparticles.

In order to support this hypothesis, we've made comparison of the results of luminescent spectroscopy with the results of IR spectroscopy (Fig. 22). There are several works [57], [58] dedicated to theoretical calculations and their comparison with experimentally obtained IR spectra of tryptophan. Unfortunately, results of these calculations are not always reliable and sometimes contradictive, therefore, deriving of definitive structural data from these measurements is not always possible. The task is even more complicated due to the fact that very few bands on the tryptophan spectrum belong to individual vibrations, most are result of a superposition of several vibrations. Nevertheless, we were able to find certain features in the region 1200-1400 cm^{-1}, in which a lot of bands associated with pyrrole ring vibrations are located (Fig. 23). Bands widening (1410 and

1585 cm^{-1}), appearance of new bands (1500 cm^{-1} for sample treated with CeO_2 (+) nanoparticles) and weakening of existing bands (1661 cm^{-1}) allows us to consider, that certain structural changes took place. Appearance of the wide bands around 3200-3300 cm^{-1} (Fig. 22) may be a result of dimerization, as bands in this region is usually associated with intermolecular vibrations or formation of larger structures [57].

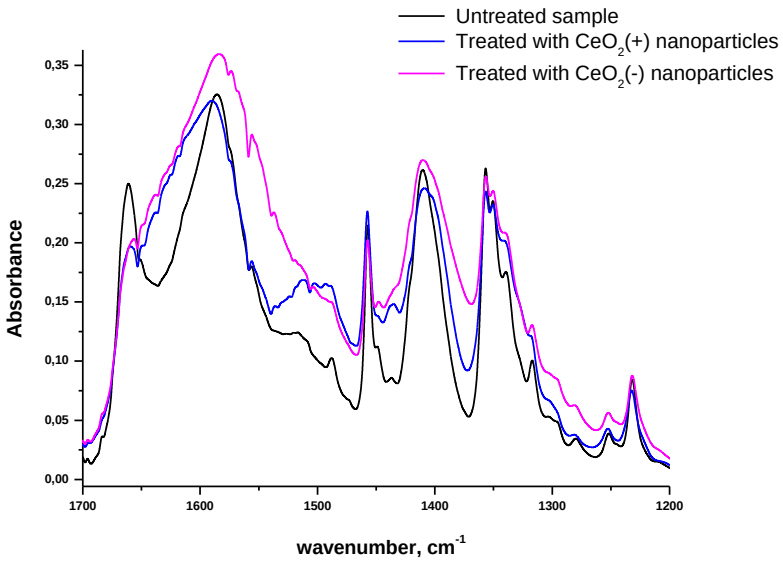

Figure 23. Enlarged part of IR spectra of untreated tryptophan and tryptophan treated with CeO_2 nanoparticles.

However, for full understanding of the nature of these changes additional research is necessary, which is out of the scope of current work. Interesting, that many of the observed changes in IR spectrum of sample treated with positively charged CeO_2 nanoparticles can be found also in the sample treated with negatively charged colloid of CeO_2, which didn't seem to affect the emission spectrum of the tryptophan, only excitation. Thus, changes in IR spectra and, therefore, molecular structure, have more correlations with excitation, than emission spectra of tryptophan luminescence. Treatment with silver nanoparticles, the same as in case of alanine, lead to some changes in bands (Fig. 24), related to carboxyl group (red shift of several bands, changes in relative intensity, appearance of new band at 834 cm^{-1}, disappearance of a band around 1515 cm^{-1}) and most likely also is connected to salt formation.

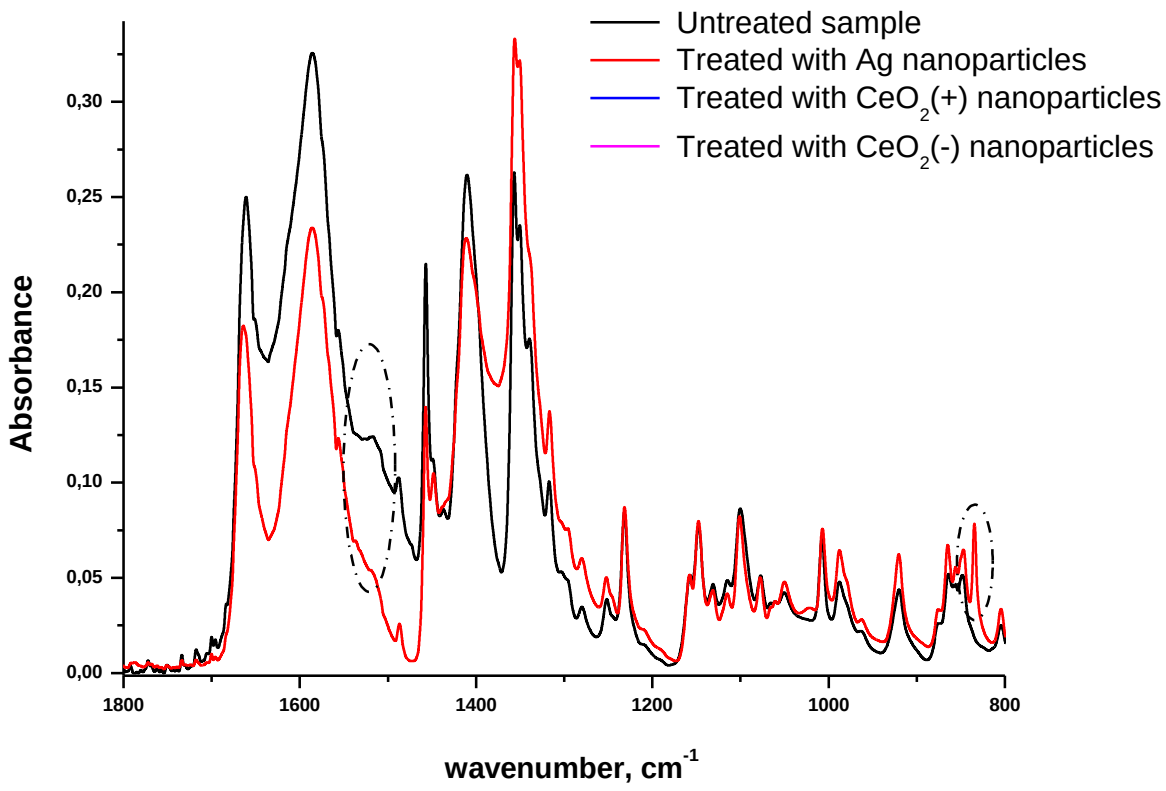

Figure 24. Enlarged part of IR spectra of untreated tryptophan and tryptophan treated with Ag nanoparticles.

In case of histidine (Fig. 25) the results of luminescent studies are a bit different.

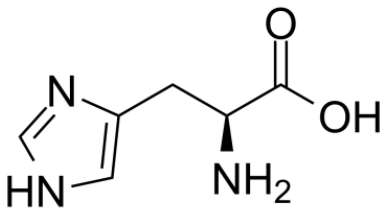

Fig 25. Structure of an L-histidine molecule.

We also observed red shift for emission spectrum of the sample treated with positively charged CeO_2 nanoparticles, but comparing to tryptophan the shift is much smaller (around 7 nm for 360 nm band and around 14 nm for 690 nm band, which both correspond

to approximately 0.05 eV shift of energy levels). On the other hand, in excitation spectra for samples treated with both positively and negatively charged CeO_2 nanoparticles appears a second band (shoulder) with higher energy (around 260 nm). It is noteworthy, that for sample treated with negatively charged CeO_2 this band is even more pronounced. However, this does not lead to any changes in the emission spectrum, allowing to suggest, that the second excitation band is related to a higher excited state, that non-radiatively relaxes to the same lower excited state, from which emission is observed. The reason of appearance of the higher excited state is unclear, but possibly it also is related to some structural changes caused by treatment of histidine solution with colloidal ceria. Unfortunately, there's not so much studies of histidine luminescence [59], [60] Partially this is due to the fact, that in proteins histidine luminescence is rarely observed, as in most cases excitation of histidine is non-radiatively transferred to tryptophan, which is emitting in lower wavelength range. On the other hand, the amount of studied luminescent derivatives of imidazole is overwhelming [61], exhibiting fluorescence in whole range from UV to NIR, so it's hard to be sure, what structural transformations could lead to the observed changes. Luminescence of imidazoles is known to be strongly pH-dependent, so we can't exclude possibility of protonation or de-protonation, but additional studies are definitely necessary.

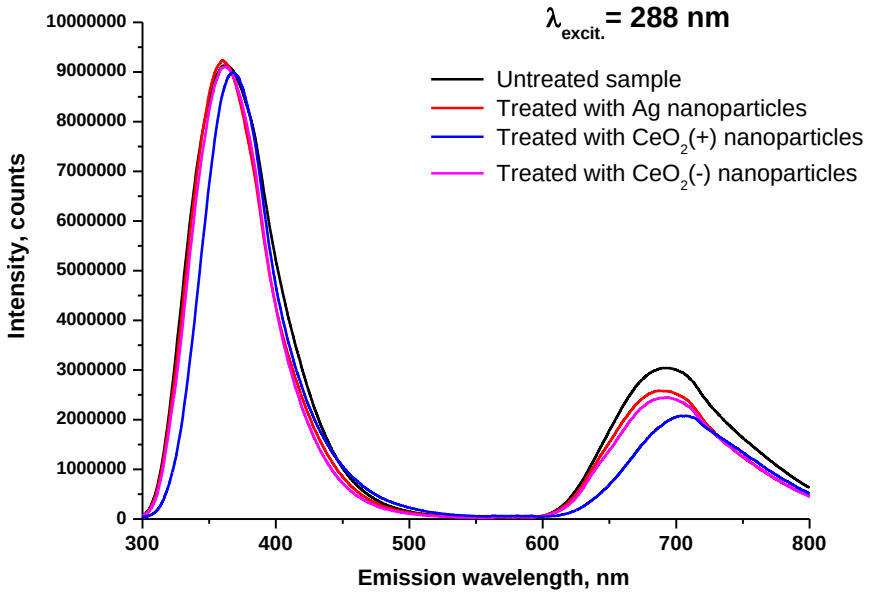

a)

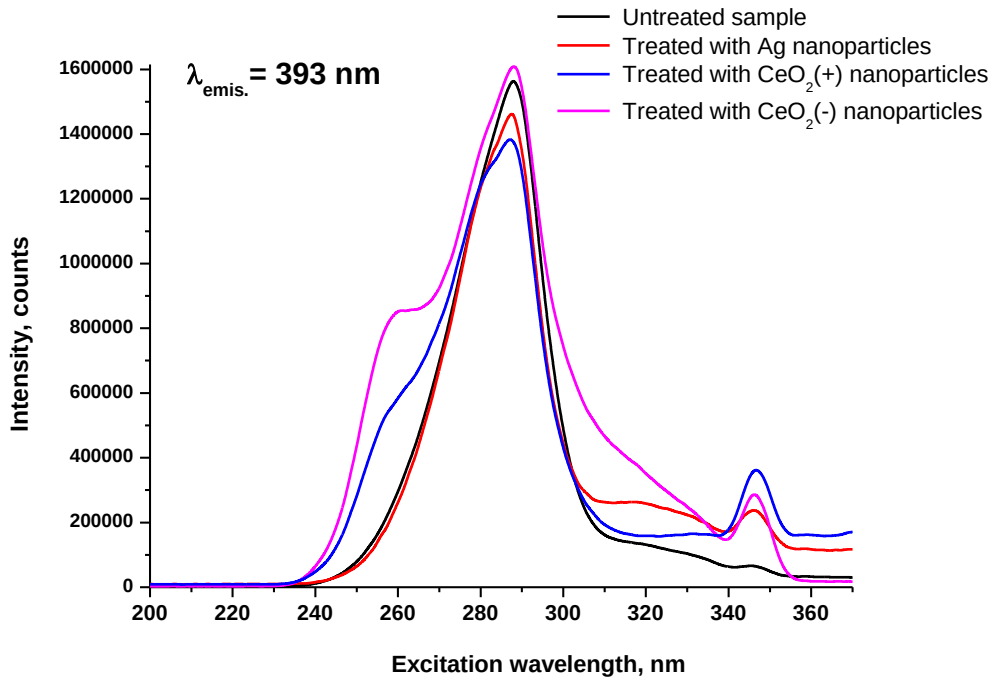

b)

Figure 26. Emission (a) and excitation (b) luminescence spectra of untreated histidine and histidine treated with synthesized nanoparticles.

Comparison of the luminescent spectra (Fig. 26) with the IR spectra (Fig. 27) leads to the same conclusions as in the case of tryptophan. The results of theoretical calculations and their comparison with experimentally obtained IR spectra [62], [63] are also inconclusive and partially contradictive in the different papers, but there are certain differences (Fig. 28) in the spectra of untreated samples and samples treated with ceria colloids (mostly for positively charged, but for negatively charged also). According to existing information in the literature, these changes are also most likely connected with vibrations of heterocycle in the molecule of amino acid. Treatment with silver nanoparticles, again, lead to some changes in bands (fig. 30), related to carboxyl group (red shift of 844 band, changes of intensity of several bands) and most likely also is connected to salt formation.

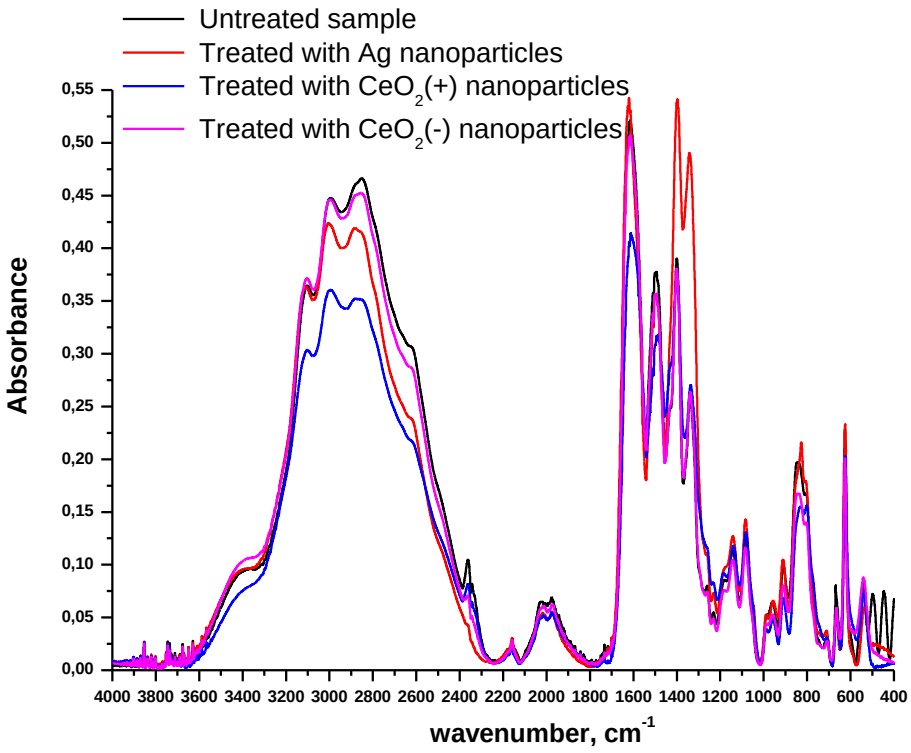

Figure 27. IR spectra of untreated histidine and histidine treated with synthesized nanoparticles.

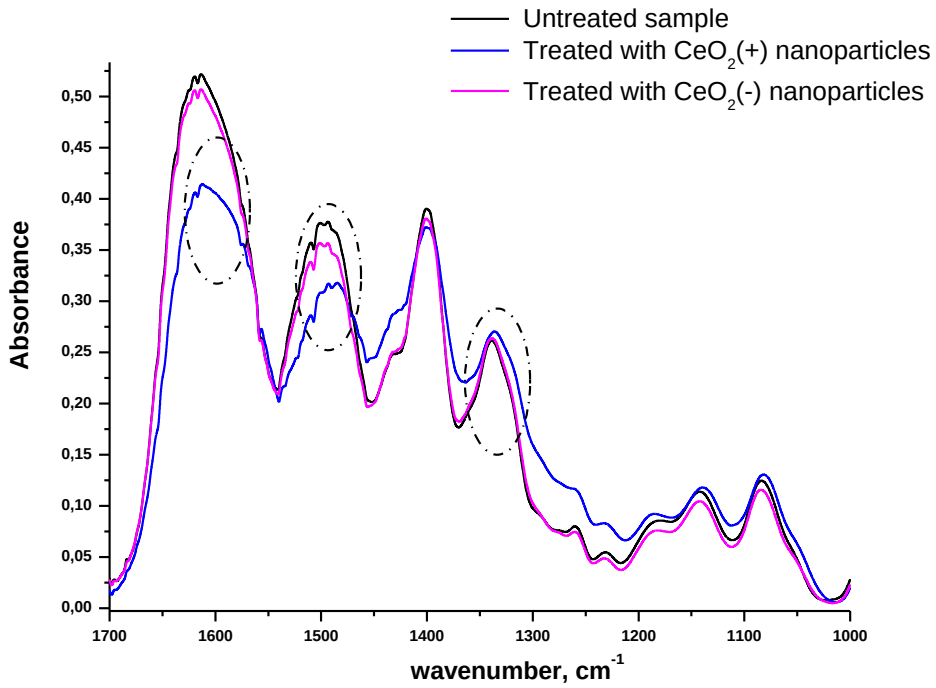

Figure 28. Enlarged part of IR spectra of untreated histidine and histidine treated with CeO_2 nanoparticles

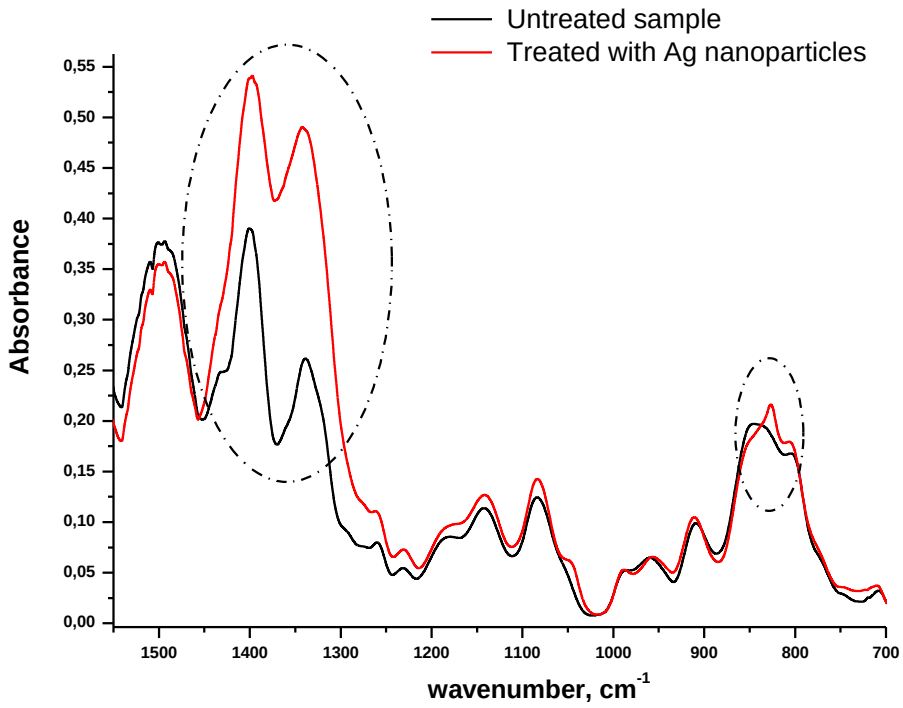

Figure 29. Enlarged part of IR spectra of untreated histidine and histidine treated with Ag nanoparticles.

Thus, the main result of comparison of the results of IR and luminescent spectroscopy of amino acids untreated and treated with synthesized nanoparticles are the following: 1) treatment with silver nanoparticles leads to formation of silver salts of corresponding amino acids, which manifests in a red shift of several bands in IR spectra, connected with carboxyl group. No visible effect on luminescence is observed. 2) treatment with both positively and negatively charged CeO_2 nanoparticles have no effect on the main functional groups of amino acids (alanine IR spectrum is not changed at all), but leads to certain structural changes in the case of amino acids with heterocycles in the structure. Nature of this effects requires further investigation, but they are irreversible – do not disappear when the CeO_2 nanoparticles are removed, 3) effects observed in IR spectra of tryptophan and histidine after treatment with nanocrystalline ceria can be correlated with the excitation spectra of the treated compounds, but not the emission spectra, which are affected only after treatment with positively charged ceria nanoparticles.

3.3.2. BSA protein measurements after treatment with positively charged CeO_2 nanoparticles

When studying proteins with IR, we can generally separate the molecule into two parts, the sidechains and the backbone. Sidechains are generally amino acids and often contribute the most to the functionality of the protein. The backbone is harder to analyze, because there are more overlapping vibrations. The problem came when trying to interpret and assign differences in the spectra to certain functional groups. Because the protein molecule is quite complex, the measured spectra bands are the result of multiple vibrations overlapping with each other. Therefore, it was impossible to derive any definitive information by comparing IR spectra of BSA before and after treatment with synthesized nanoparticles, as affected bands were impossible to assign to certain functional groups or certain amino acids, that protein molecule is containing in its structure.

However, when mixing BSA with the positive CeO_2 nanoparticles colloid, we observed a visual difference before and after treatment: the initially pink BSA solution turned white and a milky precipitate appeared. This did not happen after treatment of BSA solution with any other synthesized particles.

Therefore, we measured the circular dichroism spectra of BSA before and after treatment, which provides information about protein high order structures. Circular dichroism was measured only with positive cerium particles, as we didn't have the opportunity to measure other samples. From the CD spectra (Fig. 30) we can see degradation of the alpha-helix secondary structure into something resembling what we previously called a "random coil" structure (see Fig. 5). This coincides with our observation of the pink BSA solution turning milky when it comes into contact with positive ceria colloid. From this we can assume that positive CeO_2 nanoparticles are for some reason destroying the ordered structure of BSA protein molecules. However, nature of this effect requires additional studies, which are out of the scope of present work.

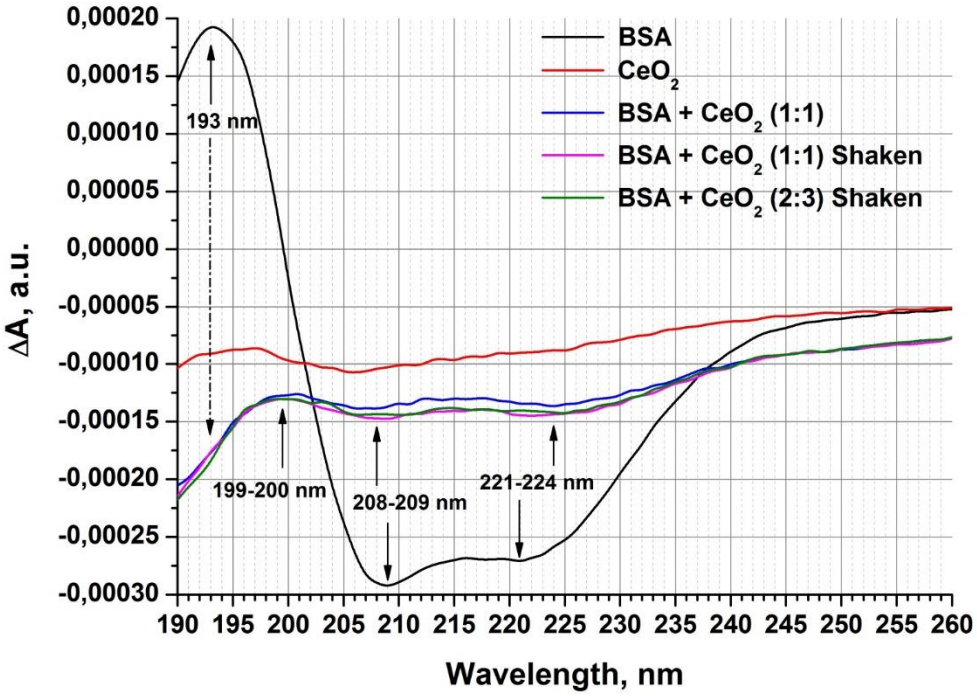

Figure 30. Circular dichroism of BSA mixed with positive nanoceria colloid, 1:1 and 2:3 show the ratio of BSA to ceria.

3.4. Antiviral testing of synthesized nanoparticles

For antiviral experiments the influenza virus A/WSN/1933 (H1N1) was selected, as a common virus with an active transmission via non-biological surfaces (clothes, furniture, common use surfaces etc.). Infected cell culture was Madin-Darby Canine Kidney cells. The antiviral experiments were performed using plaque assays. Plaques are transparent spots that are left when a dyed cell is destroyed by a virus. From this by visual counting of plaques it is possible to compare infectivity of viruses before and after treatment with synthesized nanoparticles. The testing was done with different concentrations of particles to analyze the concentration dependence of antiviral activity of synthesized nanoparticles. General appearance of plaque assays is presented on the image below (Fig. 31). The wells, uniformly covered with a dye with colorless dots (plaques), are considered successful experiments, the wells with large colorless spots are overdried and excluded from evaluations.

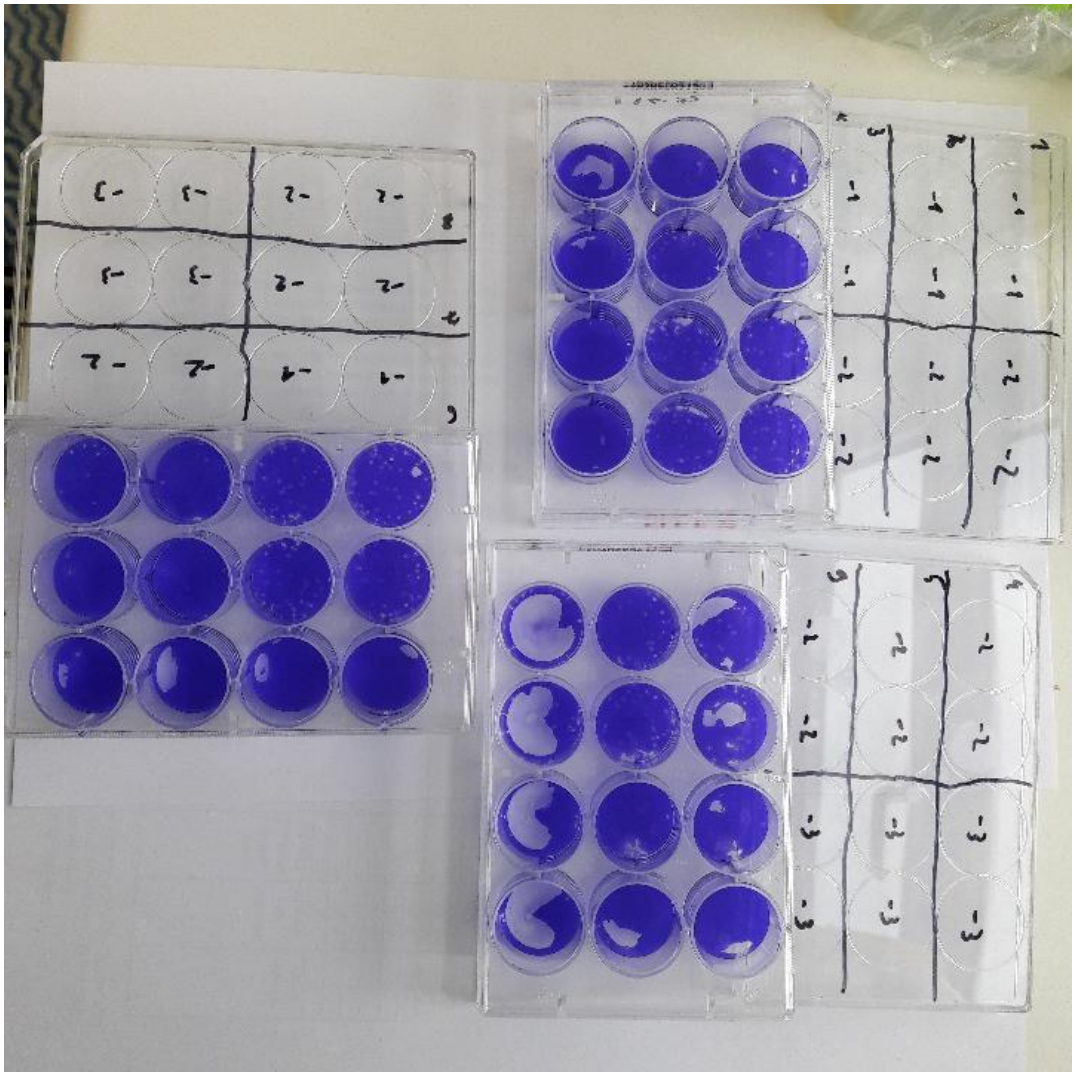

Figure 31. Dyed cells with plaques from the virus.

In parallel with antivirus experiments we performed cytotoxicity tests in human cells in order to establish the effect of synthesized nanoparticles on the cell culture. All the tested particles showed no cytotoxicity towards mammalian cells, specifically Madin-Darby Canine Kidney cells derived from canine kidney (Fig. 32). The cells were incubated with particles for up to 120 mins. Concentrations used were 0,2 mg/l, 2 mg/L and 20 mg/L for silver particles and 20 mg/L, 200 mg/L and 2000 mg/L for ceria particles.

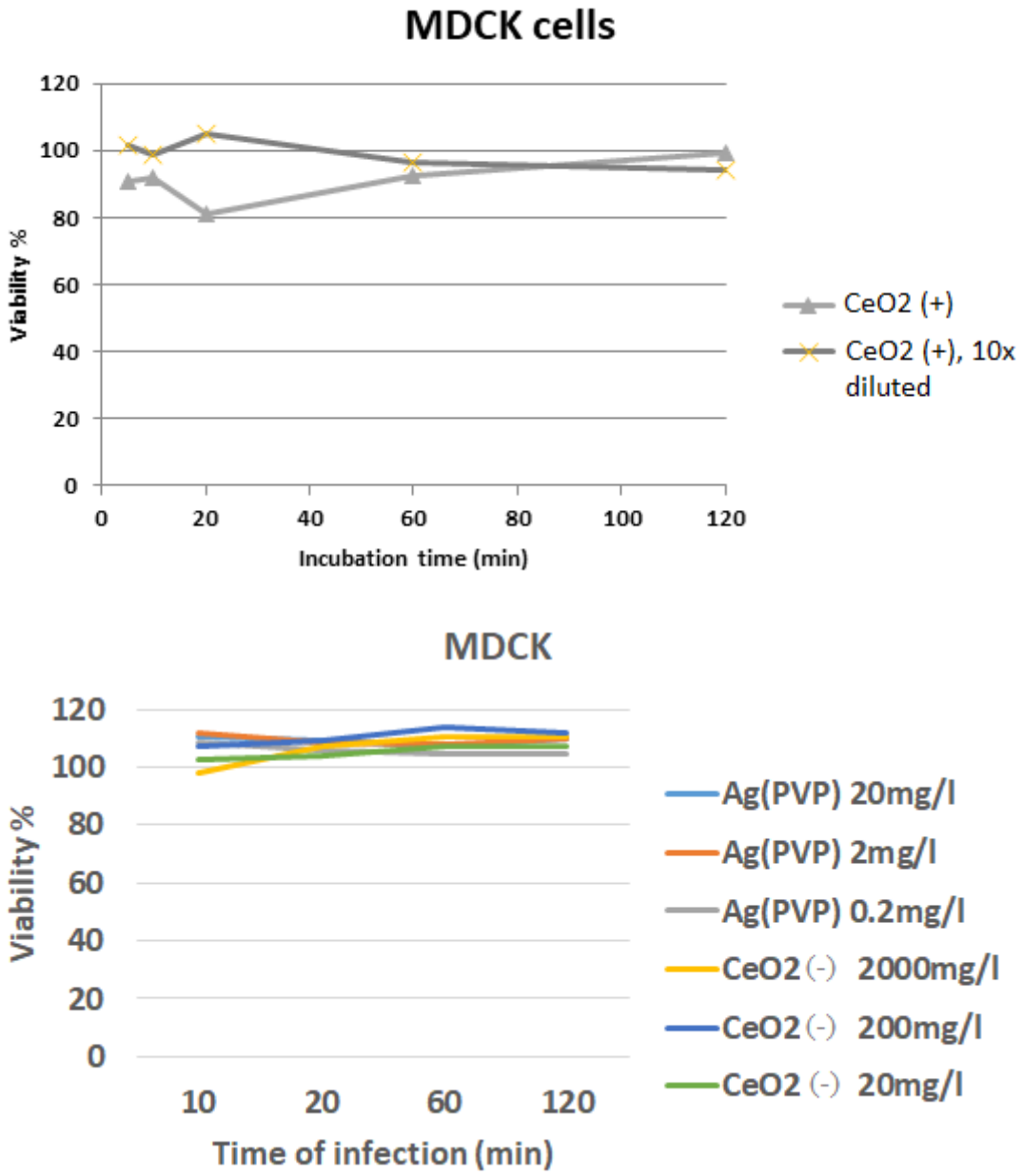

Figure 32. Cytotoxicity tests with various concentrations of silver and CeO_2 nanoparticles on MDCK cells.

Tests of infectivity of influenza virus A/WSN/1933 (H1N1) after treatment with synthesized nanoparticles (Fig. 33) showed that silver nanoparticles have only negligibly low antiviral efficiency at highest concentration (20 mg/L).

The positive ceria particles start exhibiting a minor antiviral effect at around 2 mg/L and reach close to 100% antiviral efficiency at concentration 20 mg/L. The values of

infectivity higher than 100% is due to the fact, that infectivity inhibition is compared with a control sample (virus in a media without nanoparticles) and the viability of virus even in a pure media is not always full.

The negative ceria particles are exhibiting a stronger antiviral effect at the 2 mg/L concentration, but also reach close to 100% antiviral efficiency only at concentration 20 mg/L. Which makes both types of the synthesized CeO_2 nanoparticles very promising materials for antiviral treatment of surfaces, as they combine low toxicity with high antiviral efficiency.

As we showed in previous section, CeO_2 nanoparticles exert specific effect on amino acids, as well as on protein structure. However, nature of this effect requires additional investigation, which will allow to understand and probably enhance the antiviral efficiency of CeO_2 nanoparticles.

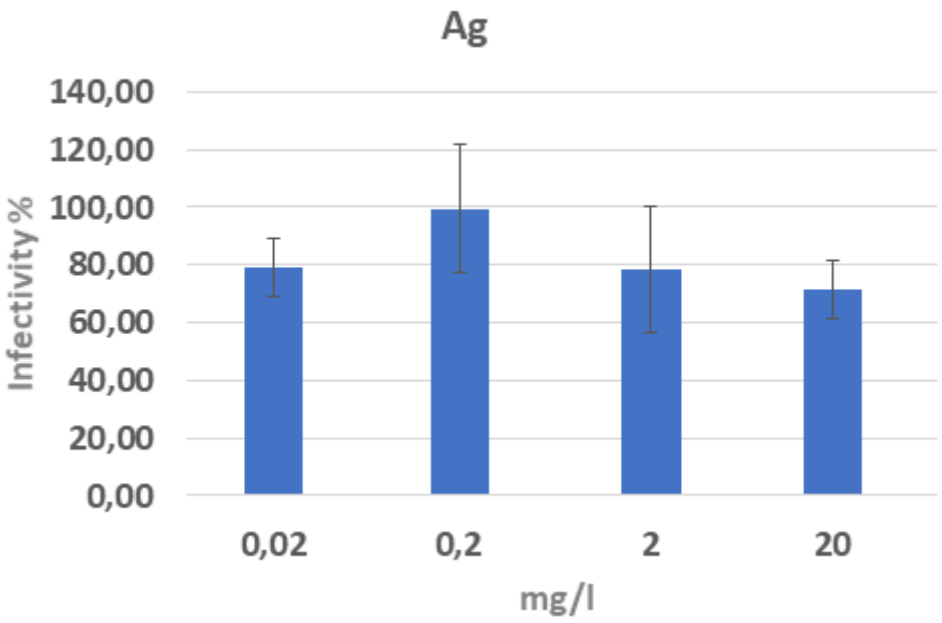

a)

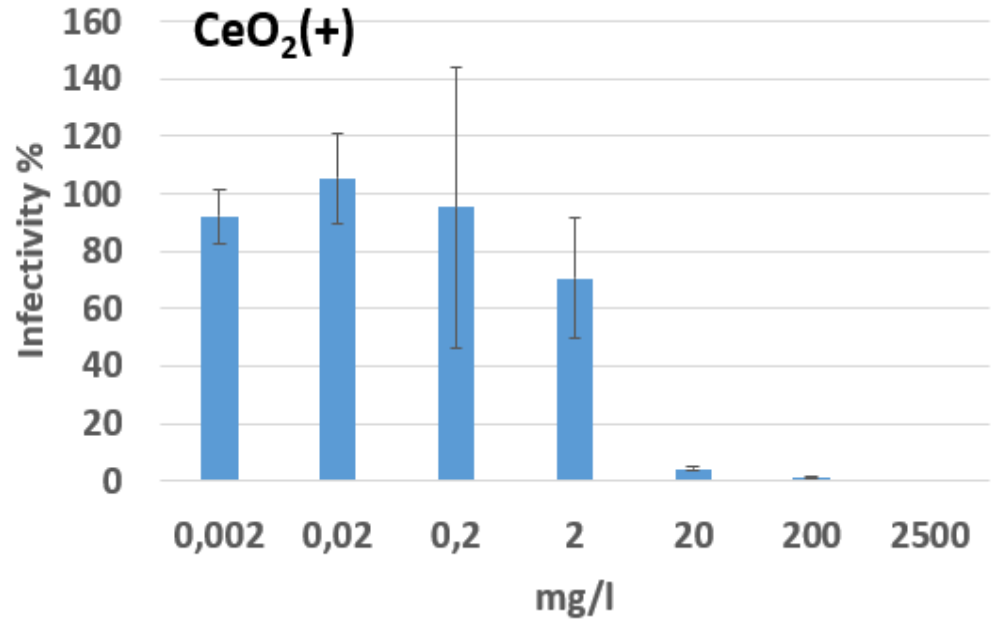

b)

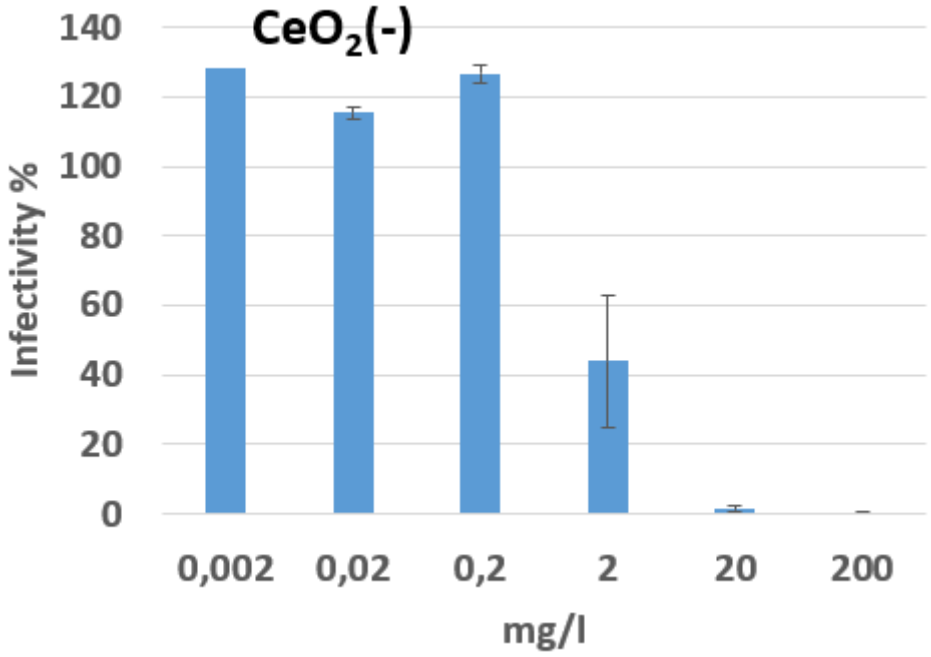

c)

Figure 33. Infectivity of WSN virus against MDCK cells treated with a) silver particles b) positive CeO_2 c) negative CeO_2.

4. Conclusions

1. Synthetic approaches for preparation of stable aqueous colloids of silver and CeO_2 nanoparticles were developed. Nanoparticle composition, morphology and surface state were characterized. It was shown, that proposed synthetic techniques allows to obtain small (<20 nm) nanoparticles of silver and ultrasmall (<10 nm) nanoparticles of CeO_2 with uniform morphology, narrow size distribution and high surface charge. Proposed techniques are easily scalable, they do not require special equipment and are suitable for commercial use.
2. Simple methods for nanoparticles distribution on various fabrics and porous surfaces were developed and tested. Feather materials commonly used for cushion filling, was submerged into Ag nanoparticle colloid solution. The uniform distribution of particles was proved by means of SEM. In most of the other tested fabric materials it was impossible to distinguish microscopically the deposited nanoparticles from the surface roughness of the said materials.
3. Effects of silver and CeO_2 nanoparticles on model bioactive compounds (amino acids and BSA protein) were studied. It was shown, that the action of silver nanoparticles was mainly connected with the dissolved Ag^+ ions, while the action of CeO_2 nanoparticles is of a more complex nature, affecting the structure of the treated compounds, and requires additional investigations.
4. Antiviral properties of synthesized compounds against influenza virus A/WSN/1933 (H1N1) were investigated using plaque-based assays in parallel with cytotoxicity studies. It was shown, that synthesized silver nanoparticles show very weak or no antiviral properties. CeO_2 nanoparticles, on the contrary, combine extremely low cytotoxicity with strong antiviral activity and have a good potential as components for externally used antiviral agents.

5. Kokkuvõte

1. Arendati välja meetodid stabiilsete hõbeda ja CeO_2 kolloidlahuste sünteesiks. Karakteriseeriti sünteesitud nanoosakeste koostis, morfoloogia ja pinnaomadused. Sünteesitud hõbeda nanoosakesed olid suurusega alla 20 nm ja CeO_2 nanoosakesed suurusega alla ’10nm. Osakestel oli ühtlane morfoloogia, kitsas suuruste jaotus ja kõrge pinnalaeng. Sünteesiks kasutatud meetodid on kergesti skaleeritavad, ei vaja erivahendeid ja on sobilikud kommertskasutuseks.
2. Arendati ja uuriti meetodeid nanoosakeste jaotamiseks kangastele ja poorsetele pindadele. Patjade täitmiseks mõeldud sulgi sukeldati hõbeda kolloid lahusesse ja kasutades SEM’i, oli nendel võimalik näha ühtlase jaotusega osakesi. Ülejäänud uuritud kangaste puhul ei olnud võimalik SEM’i kasutades nanoosakesi kanga pinnast eristada.
3. Uuriti hõbeda ja CeO_2 mõju bioaktiivsetele ühenditele (aminohapped ja BSA valk). Näidati, et hõbeda nanoosakeste mõju on peamiselt seotud lahustunud Ag^+ iooniga. Saadud tulemus on heas kooskõlas varasemate tulemustega. CeO_2 mõju osutus keerulisemaks. Antud töös näidati, et CeO2 osakesed mõjutavad aminohappe trüptofaan struktuuri. Osakeste täpsem mõjumehhanism vajab edasist uurimist.
4. Sünteesitud osakeste viirusevastase toime uurimisel kasutati gripiviirust A/WSN/1933 (H1N1). Toime uurimiseks kasutati plaagidel põhinevat analüüsi koos tsütotoksilisuse mõõtmistega. Hõbeda nanoosakestel olid nõrgad viirusevastased omadused. CeO_2-l oli vastupidiselt madal tsütotoksilisus ja tugev viirusevastane toime, mis muudab selle potentsiaalselt sobilikuks komponendiks kasutuses kehavälise viirusevastase materjalina, näiteks nahal ja limaskestadel.

Author's contribution

The author synthesized all the particles used in this work. Performed IR and luminescence spectroscopy measurements. The author was present at UV-Vis and CD spectrometry, DLS and zeta-potential measurements and analyzed the data. The author took part in one antiviral plaque assay experiment.

Acknowledgements

I would like to thank my supervisors dr. Tanel Tätte and dr. Alexander Vanetsev for their help with everything. Dr. Meeri Visnapuu for providing SEM and TEM measurements and teaching me how to use IR and UV-Vis spectrometers. Ms. Kai Rausalu and ms. Merilin Rosenberg for providing measurements with viruses and bacteria. Prof. Angela Ivask for help with analysis of anti-viral experiments. Ms. Alexandra Nefedova for help with DLS measurements. Dr. Eva Žusinaite for providing with the samples of BSA and amino acids. Dr. Mihkel Rähn for HR TEM measurements.

References

[1] V. Cagno *et al.*, “Broad-spectrum non-toxic antiviral nanoparticles with a virucidal inhibition mechanism,” *Nat. Mater.*, vol. 17, no. 2, Art. no. 2, Feb. 2018, doi: 10.1038/nmat5053.

[2] S. S. Jeremiah, K. Miyakawa, T. Morita, Y. Yamaoka, and A. Ryo, “Potent antiviral effect of silver nanoparticles on SARS-CoV-2,” *Biochem. Biophys. Res. Commun.*, vol. 533, no. 1, pp. 195–200, Nov. 2020, doi: 10.1016/j.bbrc.2020.09.018.

[3] N. M. Zholobak, Z. M. Olevinskaia, N. I. Spivak, A. B. Shcherbakov, V. K. Ivanov, and A. V. Usatenko, “[Antiviral effect of cerium dioxide nanoparticles stabilized by low-molecular polyacrylic acid],” *Mikrobiolohichnyi Zhurnal Kiev Ukr. 1993*, vol. 72, no. 3, pp. 42–47, Jun. 2010.

[4] J. A. Creighton and D. G. Eadon, “Ultraviolet–visible absorption spectra of the colloidal metallic elements,” *J Chem Soc Faraday Trans*, vol. 87, no. 24, pp. 3881–3891, 1991, doi: 10.1039/FT9918703881.

[5] K.-C. Lee, S.-J. Lin, C.-H. Lin, C.-S. Tsai, and Y.-J. Lu, “Size effect of Ag nanoparticles on surface plasmon resonance,” *Surf. Coat. Technol.*, vol. 202, no. 22, pp. 5339–5342, Aug. 2008, doi: 10.1016/j.surfcoat.2008.06.080.

[6] N. S. Abadeer and C. J. Murphy, “Recent Progress in Cancer Thermal Therapy Using Gold Nanoparticles,” *J. Phys. Chem. C*, vol. 120, no. 9, pp. 4691–4716, Mar. 2016, doi: 10.1021/acs.jpcc.5b11232.

[7] J. Turkevich, P. C. Stevenson, and J. Hillier, “A study of the nucleation and growth processes in the synthesis of colloidal gold,” *Discuss. Faraday Soc.*, vol. 11, p. 55, 1951, doi: 10.1039/df9511100055.

[8] Z. S. Pillai and P. V. Kamat, “What Factors Control the Size and Shape of Silver Nanoparticles in the Citrate Ion Reduction Method?,” *J. Phys. Chem. B*, vol. 108, no. 3, pp. 945–951, Jan. 2004, doi: 10.1021/jp037018r.

[9] A. Pyatenko, M. Yamaguchi, and M. Suzuki, “Synthesis of Spherical Silver Nanoparticles with Controllable Sizes in Aqueous Solutions,” *J. Phys. Chem. C*, vol. 111, no. 22, pp. 7910–7917, Jun. 2007, doi: 10.1021/jp071080x.

[10] I. Sondi and B. Salopek-Sondi, “Silver nanoparticles as antimicrobial agent: a case study on E. coli as a model for Gram-negative bacteria,” *J. Colloid Interface Sci.*, vol. 275, no. 1, pp. 177–182, Jul. 2004, doi: 10.1016/j.jcis.2004.02.012.

[11] W.-R. Li, X.-B. Xie, Q.-S. Shi, H.-Y. Zeng, Y.-S. OU-Yang, and Y.-B. Chen, “Antibacterial activity and mechanism of silver nanoparticles on Escherichia coli,” *Appl. Microbiol. Biotechnol.*, vol. 85, no. 4, pp. 1115–1122, Jan. 2010, doi: 10.1007/s00253-009-2159-5.

[12] H. Xu *et al.*, “Role of reactive oxygen species in the antibacterial mechanism of silver nanoparticles on Escherichia coli O157:H7,” *BioMetals*, vol. 25, no. 1, pp. 45–53, Feb. 2012, doi: 10.1007/s10534-011-9482-x.

[13] B. Le Ouay and F. Stellacci, “Antibacterial activity of silver nanoparticles: A surface science insight,” *Nano Today*, vol. 10, no. 3, pp. 339–354, Jun. 2015, doi: 10.1016/j.nantod.2015.04.002.

[14] P. Dutta, S. Pal, M. S. Seehra, Y. Shi, E. M. Eyring, and R. D. Ernst, “Concentration of Ce $^{3+}$ and Oxygen Vacancies in Cerium Oxide Nanoparticles,” *Chem. Mater.*, vol. 18, no. 21, pp. 5144–5146, Oct. 2006, doi: 10.1021/cm061580n.

[15] M. Hijaz *et al.*, “Folic acid tagged nanoceria as a novel therapeutic agent in ovarian cancer,” *BMC Cancer*, vol. 16, Mar. 2016, doi: 10.1186/s12885-016-2206-4.

[16] J. Paier, C. Penschke, and J. Sauer, “Oxygen Defects and Surface Chemistry of Ceria: Quantum Chemical Studies Compared to Experiment,” *Chem. Rev.*, vol. 113, no. 6, pp. 3949–3985, Jun. 2013, doi: 10.1021/cr3004949.

[17] T. Xia *et al.*, “Comparison of the abilities of ambient and manufactured nanoparticles to induce cellular toxicity according to an oxidative stress paradigm,” *Nano Lett.*, vol. 6, no. 8, pp. 1794–1807, Aug. 2006, doi: 10.1021/nl061025k.

[18] E. Burello and A. P. Worth, “A theoretical framework for predicting the oxidative stress potential of oxide nanoparticles,” *Nanotoxicology*, vol. 5, no. 2, pp. 228–235, Jun. 2011, doi: 10.3109/17435390.2010.502980.

[19] X. Hao *et al.*, *Cerium Valence State Distribution: Atomic-Scale Valence State Distribution inside Ultrafine CeO2 Nanocubes and Its Size Dependence (Small 42/2018)*, vol. 14. 2018. doi: 10.1002/smll.201870195.

[20] N. Thakur, P. Manna, and J. Das, “Synthesis and biomedical applications of nanoceria, a redox active nanoparticle,” *J. Nanobiotechnology*, vol. 17, no. 1, p. 84, Jul. 2019, doi: 10.1186/s12951-019-0516-9.

[21] T. Sahu, S. Bisht, K. Das, and S. Kerkar, “Nanoceria: Synthesis and Biomedical Applications,” *Curr. Nanosci.*, vol. 9, Jul. 2013, doi: 10.2174/15734137113099990084.

[22] H. Li, Z. Wang, L. Chen, and X. Huang, “Synthesis and Characterization of Polycrystalline CeO2 Nanowires,” *Chem. Lett. - CHEM LETT*, vol. 33, pp. 662–663, Jun. 2004, doi: 10.1246/cl.2004.662.

[23] T. Masui, H. Hirai, N. Imanaka, G. Adachi, T. Sakata, and H. Mori, “Synthesis of cerium oxide nanoparticles by hydrothermal crystallization with citric acid,” *J. Mater. Sci. Lett.*, vol. 21, no. 6, pp. 489–491, Mar. 2002, doi: 10.1023/A:1015342925372.

[24] B. Hanafy, G. Cave, Y. Barnett, and B. Pierscionek, “Ethylene glycol coated nanoceria protects against oxidative stress in human lens epithelium,” *RSC Adv.*, vol. 9, pp. 16596–16605, Jan. 2019, doi: 10.1039/C9RA01252D.

[25] A. Dhall and W. Self, “Cerium Oxide Nanoparticles: A Brief Review of Their Synthesis Methods and Biomedical Applications,” *Antioxid. Basel Switz.*, vol. 7, no. 8, Jul. 2018, doi: 10.3390/antiox7080097.

[26] H. E. A. Mohamed *et al.*, “Promising antiviral, antimicrobial and therapeutic properties of green nanoceria,” *Nanomed.*, vol. 15, no. 5, pp. 467–488, Feb. 2020, doi: 10.2217/nnm-2019-0368.

[27] J.-S. Lee and S.-C. Choi, “Crystallization behavior of nano-ceria powders by hydrothermal synthesis using a mixture of H2O2 and NH4OH,” *Mater. Lett.*, vol. 58, no. 3, pp. 390–393, Jan. 2004, doi: 10.1016/S0167-577X(03)00508-1.

[28] N. J. Rogers *et al.*, “Physico-chemical behaviour and algal toxicity of nanoparticulate CeO2 in freshwater,” *Environ. Chem.*, vol. 7, no. 1, pp. 50–60, Feb. 2010, doi: 10.1071/EN09123.

[29] I. Rodea-Palomares *et al.*, “Physicochemical Characterization and Ecotoxicological Assessment of CeO2 Nanoparticles Using Two Aquatic Microorganisms,” *Toxicol. Sci. Off. J. Soc. Toxicol.*, vol. 119, pp. 135–45, Oct. 2010, doi: 10.1093/toxsci/kfq311.

[30] K. V. Hoecke *et al.*, “Fate and Effects of CeO $_2$ Nanoparticles in Aquatic Ecotoxicity Tests,” *Environ. Sci. Technol.*, vol. 43, no. 12, pp. 4537–4546, Jun. 2009, doi: 10.1021/es9002444.

[31] S. Lin *et al.*, “Aspect Ratio Plays a Role in the Hazard Potential of CeO2 Nanoparticles in Mouse Lung and Zebrafish Gastrointestinal Tract,” *ACS Nano*, vol. 8, no. 5, pp. 4450–4464, May 2014, doi: 10.1021/nn5012754.

[32] G. Pulido-Reyes *et al.*, “Untangling the biological effects of cerium oxide nanoparticles: the role of surface valence states,” *Sci. Rep.*, vol. 5, no. 1, p. 15613, Dec. 2015, doi: 10.1038/srep15613.

[33] S. Burkes and C. S. Mccleskey, “The Bacteriostatic Activity of Cerium, Lanthanum, and Thallium,” *J. Bacteriol.*, vol. 54, no. 4, pp. 417–424, Oct. 1947.

[34] J. P. Garner and P. S. J. Heppell, “Cerium nitrate in the management of burns,” *Burns*, vol. 31, no. 5, pp. 539–547, Aug. 2005, doi: 10.1016/j.burns.2005.01.014.

[35] W. Lin, Y. Huang, X.-D. Zhou, and Y. Ma, “Toxicity of Cerium Oxide Nanoparticles in Human Lung Cancer Cells,” *Int. J. Toxicol.*, vol. 25, no. 6, pp. 451–457, Nov. 2006, doi: 10.1080/10915810600959543.

[36] S. Singh, “Cerium oxide based nanozymes: Redox phenomenon at biointerfaces,” *Biointerphases*, vol. 11, no. 4, p. 04B202, Nov. 2016, doi: 10.1116/1.4966535.

[37] A. TROVARELLI, “Catalytic Properties of Ceria and CeO2-Containing Materials,” *Catal. Rev.*, vol. 38, no. 4, pp. 439–520, Nov. 1996, doi: 10.1080/01614949608006464.

[38] A. Popov *et al.*, “Radioprotective effects of ultra-small citrate-stabilized cerium oxide nanoparticles in vitro and in vivo,” *RSC Adv.*, vol. 6, Oct. 2016, doi: 10.1039/C6RA18566E.

[39] A. Barth, “Infrared spectroscopy of proteins,” *Biochim. Biophys. Acta BBA - Bioenerg.*, vol. 1767, no. 9, pp. 1073–1101, Sep. 2007, doi: 10.1016/j.bbabio.2007.06.004.

[40] A. Maeda, “Application of FTIR Spectroscopy to the Structural Study on the Function of Bacteriorhodopsin,” *Isr. J. Chem.*, vol. 35, no. 3–4, pp. 387–400, 1995, doi: https://doi.org/10.1002/ijch.199500038.

[41] D. Thoenges and A. Barth, “Direct Measurement of Enzyme Activity with Infrared Spectroscopy,” *J. Biomol. Screen.*, vol. 7, pp. 353–7, Sep. 2002, doi: 10.1089/108705702320351204.

[42] M. Hospes, J. Hendriks, and K. J. Hellingwerf, “Tryptophan fluorescence as a reporter for structural changes in photoactive yellow protein elicited by photo-activation,” *Photochem Photobiol Sci*, vol. 12, no. 3, pp. 479–488, 2013, doi: 10.1039/C2PP25222H.

[43] W. C. Johnson, “Protein secondary structure and circular dichroism: A practical guide,” *Proteins Struct. Funct. Bioinforma.*, vol. 7, no. 3, pp. 205–214, 1990, doi: https://doi.org/10.1002/prot.340070302.

[44] V. Dodero, Z. Quirolo, and A. Sequeira, “Biomolecular studies by circular dichroism,” *Front. Biosci. J. Virtual Libr.*, vol. 16, pp. 61–73, Jan. 2011, doi: 10.2741/3676.

[45] D. Aherne, D. M. Ledwith, M. Gara, and J. M. Kelly, “Optical Properties and Growth Aspects of Silver Nanoprisms Produced by a Highly Reproducible and Rapid Synthesis at Room Temperature,” *Adv. Funct. Mater.*, vol. 18, no. 14, pp. 2005–2016, 2008, doi: https://doi.org/10.1002/adfm.200800233.

[46] V. Ivanov, V. Kozik, A. Shaporev, A. Baranchikov, S. Kuznetsova, and A. Zabolotskaya, “Synthesis of the Nanopowders of CeO2 and ZnO with Controllable Particle Size by Means of Homogeneous Hydrolysis in the Presence of Hexamethylenetetramine,” vol. 19, pp. 229–236, Apr. 2011.

[47] G. Jayakumar, A. A. Irudayaraj, and A. D. Raj, “Particle Size Effect on the Properties of Cerium Oxide (CeO2) Nanoparticles Synthesized by Hydrothermal Method 30,” *Mater. Sci.*, p. 6, 2017.

[48] X. Cao and G. Fischer, “New infrared spectra and the tautomeric studies of purine and αl-alanine with an innovative sampling technique,” *Spectrochim. Acta. A. Mol. Biomol. Spectrosc.*, vol. 55, no. 11, pp. 2329–2342, Sep. 1999, doi: 10.1016/S1386-1425(99)00133-X.

[49] Е. В. Бутырская, Л. С. Нечаева, В. А. Шапошник, and В. Ф. Селеменев, “Отнесение Полос В Ик-Спектрах Водных Растворов Аланина На Основе Квантово-Химического Расчета,” *Вестник Воронежского Государственного Университета Серия Химия Биология Фармация*, no. 2, 2014.

[50] A. G. Szabo and D. M. Rayner, “Fluorescence decay of tryptophan conformers in aqueous solution,” *J. Am. Chem. Soc.*, vol. 102, no. 2, pp. 554–563, Jan. 1980, doi: 10.1021/ja00522a020.

[51] E. V. Donckt, “Fluorescence Solvent Shifts and Singlet Excited State pK’s of Indole Derivatives,” *Bull. Sociétés Chim. Belg.*, vol. 78, no. 1–2, pp. 69–75, Sep. 2010, doi: 10.1002/bscb.19690780110.

[52] G. S. Kembrovskii, V. P. Bobrovich, and S. V. Konev, “Low-temperature luminescence spectra of indole,” *J. Appl. Spectrosc.*, vol. 5, no. 5, pp. 501–503, Nov. 1966, doi: 10.1007/BF00608889.

[53] J. T. Vivian and P. R. Callis, “Mechanisms of Tryptophan Fluorescence Shifts in Proteins,” *Biophys. J.*, vol. 80, no. 5, pp. 2093–2109, May 2001, doi: 10.1016/S0006-3495(01)76183-8.

[54] C. F. Chabalowski, D. R. Garmer, J. O. Jensen, and M. Krauss, “Reaction field calculation of the spectral shifts of indole,” *J. Phys. Chem.*, vol. 97, no. 18, pp. 4608–4613, May 1993, doi: 10.1021/j100120a009.

[55] K. Radotić, T. B. Melø, R. M. Leblanc, Y. A. Yousef, and K. R. Naqvi, “Fluorescence and phosphorescence of tryptophan in peptides of different length and sequence,” *J. Photochem. Photobiol. B*, vol. 157, pp. 120–128, Apr. 2016, doi: 10.1016/j.jphotobiol.2016.02.011.

[56] A. V. Fonin, A. I. Sulatskaya, I. M. Kuznetsova, and K. K. Turoverov, “Fluorescence of Dyes in Solutions with High Absorbance. Inner Filter Effect Correction,” *PLoS ONE*, vol. 9, no. 7, p. e103878, Jul. 2014, doi: 10.1371/journal.pone.0103878.

[57] X. Cao and G. Fischer, “Infrared Spectral, Structural, and Conformational Studies of Zwitterionic L -Tryptophan,” *J. Phys. Chem. A*, vol. 103, no. 48, pp. 9995–10003, Dec. 1999, doi: 10.1021/jp992421c.

[58] Vernadsky Institute of Geochemistry and Analytical Chemistry *et al.*, “Modeling of Vibrational Spectra of L-tryptophan in Condensed States,” *Ser. Phys.*, vol. 17, no. 1, pp. 20–32, 2017, doi: 10.18500/1817-3020-2017-17-1-20-32.

[59] M. O. Iwunze, “The characterization of the fluorescence of l-histidine in simulated body fluid,” *J. Photochem. Photobiol. Chem.*, vol. 186, no. 2–3, pp. 283–289, Feb. 2007, doi: 10.1016/j.jphotochem.2006.05.034.

[60] L. Brand and S. Shaltiel, “Modification of histidine residues leading to the appearance of visible fluorescence,” *Biochim. Biophys. Acta BBA - Spec. Sect. Biophys. Subj.*, vol. 88, no. 2, pp. 338–351, Sep. 1964, doi: 10.1016/0926-6577(64)90189-5.

[61] M. Y. Berezin, J. Kao, and S. Achilefu, “pH-Dependent Optical Properties of Synthetic Fluorescent Imidazoles,” *Chem. - Eur. J.*, vol. 15, no. 14, pp. 3560–3566, Mar. 2009, doi: 10.1002/chem.200801784.

[62] J. G. Mesu, T. Visser, F. Soulimani, and B. M. Weckhuysen, “Infrared and Raman spectroscopic study of pH-induced structural changes of l-histidine in aqueous environment,” *Vib. Spectrosc.*, vol. 39, no. 1, pp. 114–125, Sep. 2005, doi: 10.1016/j.vibspec.2005.01.003.

[63] S. Kumar, A. K. Rai, S. B. Rai, and D. K. Rai, “Infrared and Raman spectra of Histidine: an ab initio DFT calculations of Histidine molecule and its different protonated forms,” *Indian J. Phys.*, vol. 84, no. 5, pp. 563–573, May 2010, doi: 10.1007/s12648-010-0039-6.

Lihtlitsents lõputöö reprodutseerimiseks ja üldsusele kättesaadavaks tegemiseks

Mina, Stevin Lilla,

1. annan Tartu Ülikoolile tasuta loa (lihtlitsentsi) minu loodud teose

_ **Synthesis of silver and cerium dioxide nanoparticles and study of their antiviral activity**,

mille juhendaja on dr Tanel Tätte, dr Alexander Vanetsev

reprodutseerimiseks eesmärgiga seda säilitada, sealhulgas lisada digitaalarhiivi DSpace kuni autoriõiguse kehtivuse lõppemiseni.

2. Annan Tartu Ülikoolile loa teha punktis 1 nimetatud teos üldsusele kättesaadavaks Tartu Ülikooli veebikeskkonna, sealhulgas digitaalarhiivi DSpace kaudu Creative Commonsi litsentsiga CC BY NC ND 3.0, mis lubab autorile viidates teost reprodutseerida, levitada ja üldsusele suunata ning keelab luua tuletatud teost ja kasutada teost ärieesmärgil, alates ***04.06.2023*** kuni autoriõiguse kehtivuse lõppemiseni.

3. Olen teadlik, et punktides 1 ja 2 nimetatud õigused jäävad alles ka autorile.

4. Kinnitan, et lihtlitsentsi andmisega ei riku ma teiste isikute intellektuaalomandi ega isikuandmete kaitse õigusaktidest tulenevaid õigusi.

Stevin Lilla

04.06.2021